AEDC-TR-71-212

Cy 1

FURTHER EVALUATION OF A NEW FACILITY CONCEPT FOR TESTING LARGE ABLATION MODELS AT HIGH STAGNATION PRESSURES

R. T. Smith and J. C. Pigott
ARO, Inc.

October 1971

Approved for public release; distribution unlimited.

PROPULSION WIND TUNNEL FACILITY
ARNOLD ENGINEERING DEVELOPMENT CENTER
AIR FORCE SYSTEMS COMMAND
ARNOLD AIR FORCE STATION, TENNESSEE

PROPERTY OF U S AIR FORCE
AEDC LIBRARY
F40600-72-C-0003

NOTICES

When U. S. Government drawings specifications, or other data are used for any purpose other than a definitely related Government procurement operation, the Government thereby incurs no responsibility nor any obligation whatsoever, and the fact that the Government may have formulated, furnished, or in any way supplied the said drawings, specifications, or other data, is not to be regarded by implication or otherwise, or in any manner licensing the holder or any other person or corporation, or conveying any rights or permission to manufacture, use, or sell any patented invention that may in any way be related thereto.

Qualified users may obtain copies of this report from the Defense Documentation Center.

References to named commercial products in this report are not to be considered in any sense as an endorsement of the product by the United States Air Force or the Government.

FURTHER EVALUATION OF A NEW FACILITY CONCEPT FOR TESTING LARGE ABLATION MODELS AT HIGH STAGNATION PRESSURES

R. T. Smith and J. C. Pigott
ARO, Inc.

Approved for public release; distribution unlimited.

FOREWORD

The research reported herein was sponsored by the Arnold Engineering Development Center (AEDC), Air Force Systems Command (AFSC), under Program Element 62201F, Project 8950.

The results of the research presented in this report were obtained by ARO, Inc. (a subsidiary of Sverdrup & Parcel and Associates, Inc.), contract operator of the AEDC, AFSC, Arnold Air Force Station, Tennessee, under Contract F40600-72-C-0003. The work was performed from July 1, 1970, to June 30, 1971, under ARO Project PW5103, and the manuscript submitted for publication on August 11, 1971.

The authors wish to acknowledge the work of M. D. High, ARO, Inc., who developed the approximation of the relation between heat flux and total enthalpy based on the Fay-Riddell solution for stagnation point heat transfer in laminar flow.

This technical report has been reviewed and is approved.

Ules L. Barnwell
Major, USAF
Research and Development Center
Directorate of Technology

R. O. Dietz
Acting Director of Technology
Directorate of Technology

ABSTRACT

This report presents the results of the third phase of an investigation to determine the feasibility of extending ablation test facility capability by surrounding the high enthalpy flow with a coaxial cold jet. The technique was applied to the 5-MW arc heated facility at pressures up to 80 atm. A variety of data probes and models were used to determine flow-model interactions. Final results show the technique to be excellent for simulating flow over very large ablation models.

CONTENTS

APPENDIXES

I. ILLUSTRATIONS

Figure

NOMENCLATURE

H_o	Stagnation enthalpy, Btu/lbm
M	Mach number
$\dot{m}$	Recession rate, lb/ft^2-sec
p_o	Total pressure, atm
p_o'	Stagnation point pressure, atm
$\dot{q}$	Heat flux, Btu/ft^2-sec
R_N	Model nose radius, in.
r_e	Central nozzle exit radius, 0.3468 in.
S	Distance along model surface measured from the stagnation point
x	Distance from central nozzle exit measured along the nozzle axis

SUBSCRIPTS

C	Cold shroud flow
cw	Cold wall
℄	Centerline value
Calor	Calorimeter
ESF	Computed from equilibrium sonic flow equation (Ref. 8)
H	High enthalpy flow
HB	Heat balance $\left(\frac{\text{Power In - Losses}}{\text{Air Mass Flow}}\right)$
HW	Hot wall
P	Probe
SP	Stagnation point
∞	Free stream

SECTION I
INTRODUCTION

The requirement for studying ablation and other phenomena associated with reentry has led to the development of a variety of small, high enthalpy, high pressure test facilities. The very large power requirements as well as problems encountered in developing large or multiple-arc heaters have limited the size of these facilities. Since these facilities are operated at high stagnation pressures and normally exhaust to atmospheric pressure, a nonuniform expanding flow field exists over much of the model nose, beginning with the intersection of the nozzle Mach wave with the model, as shown in Fig. 1a (Appendix I). Therefore, for nose cone ablation tests of the types recently conducted, only a limited region of uniform flow is obtained. One method of eliminating the expansion would be to place the facility and the model in a pressurized tank. However, this presents many serious operational and hardware problems.

Another possible method, as proposed in Ref. 1, is to surround the high enthalpy flow with a coaxial cold air jet with static pressures matched at the interface. The coaxial jet could eliminate the expansion at the high enthalpy nozzle exit, thereby providing the correct flow field over a much larger region of the model. This is typically shown in Fig. 1b. Also for ablation testing of blunt bodies, a proper matching of the cold airflow would impose the correct flow field over a body that is large relative to the high enthalpy flow nozzle. Valid ablation data could then be obtained until the mixing of the flows finally reduces the enthalpy of the model boundary layer. This coaxial flow technique would, therefore, improve the quality of the flow field, permit the testing of larger models, or reduce the facility power for experimental studies.

During Phase I of this investigation (Refs. 1 and 2), a warm jet of carbon dioxide, heated in an electrical resistance heater, was used to simulate the high enthalpy flow and to investigate potential problem areas as well as determine criteria for application of the coaxial flow technique to arc heaters. The objective of Phase II of this investigation was to apply the concept to an arc heater facility and thereby to determine the feasibility of the concept. Having proved feasibility, Phase III was conducted to apply the technique to a high pressure arc heater and to obtain a more comprehensive calibration of the flow at high pressure.

SECTION II
TEST APPARATUS

2.1 ABLATION FACILITY

The tests were conducted using dry air in the 5-MW Research Arc Heater (RAH). The 5-MW RAH, shown in Fig. 2, is a continuous-flow, modified, Linde N4000 arc heater, and is further described in Ref. 3. The arc heater was direct-coupled to the coaxial nozzle assembly. The heated flow was expanded through an M = 2.5 contoured nozzle (see Section 2.2) and exhausted to atmospheric pressure. Figure 3 shows the overall exterior view of the arc heater and test cell installation.

2.2 COAXIAL NOZZLE ASSEMBLY

The configuration of the coaxial flow nozzle assembly is shown in Fig. 4 and is the same nozzle used during Phase II testing. The arc-heated flow nozzle has a nominal 3/8-in. throat diameter and an exit Mach number of 2.5. The annular cold air nozzle has a nominal exit diameter of 1.6 in. and an exit Mach number of 2.36. The annular air nozzle Mach number was chosen to match the criteria given in Refs. 1 and 2 for "large blunt bodies" but does not represent the lowest Mach number that may be used. These criteria require that both the static pressures and the pitot pressure of the two flows be equal at the nozzle exits. This design gives an annular cold air mass flow of seventeen times that of the arc-heated flow when the flow pressures are matched. Both the arc heater and the annular air nozzles were designed using computer program formulation of the method of characteristics. The complete table of coordinates will not be presented here.

The annular air jet was unheated dry air at a nominal stagnation temperature of 480°R. Testing was conducted at total pressures varying from about 20 to 81 atm which resulted in nozzle exit static pressures of from 1.08 to 4.4 atm. Exploratory testing was conducted with a mismatch of the annular flow static pressure of approximately ±25 percent at a nominal arc heater pressure of 60 atm. The arc heater stagnation enthalpy varied from 2500 Btu/lbm at 20 atm to about 1900 Btu/lbm at 80 atm.

Two nozzle shroud extensions were evaluated in the test program. One was 0.8 in. long, the other 1.6 in. long. The purpose of the nozzle extensions was to increase the uniformity of the flow in the test region by providing a longer mixing length for the two jet streams and by reducing the strength of shock waves in the test region of the flow.

2.3 TEST MODELS AND INSTRUMENTATION

Several unique instrumentation techniques were used to calibrate the flow. It was very clear from the onset of the present project that typical water-cooled models and probes would not withstand the hostile environment generated by the high pressure hot gas. As a result of this, the project was run in close liaison with an ablation instrumentation development project. The probes described here were developed under that project and are described in detail in Ref. 4. The probes developed were all transient probes swept through the flow in a few milliseconds with responses recorded with dynamic instrumentation.

2.3.1 Pressure Probe

It was decided that a small pressure probe, i. e., boundary layer probe, was needed to define the mixing layer area between the two flows. The probe developed and described in Ref. 4 was used extensively in the calibration of this flow. The boundary layer probe was made of copper (for heat sink capability and strength) with a large base and a 0.075-in. nose diameter. The probe utilizes a Kistler Instrument Company Model 603A® crystal gage transducer which was close-coupled to the probe orifice so that sweep profiles were obtained within 50 msec. A photograph of the probe is shown in Fig. 5.

2.3.2 Enthalpy Probe

The transient enthalpy probe concept, as developed by Cornell Aeronautical Laboratory (Ref. 5) is unique in that it utilizes the transient temperature rise of the gas sampling tube as a measure of sample energy loss. It is protected from extraneous heat loss or gain by means of a thermal-electrical insulating air space which is located between the inside and outside tubes. This protective shield is an uncooled mass of copper which protects and insulates the sampling tube from the flow stream. The AEDC version of this probe features a fast response mass flow measuring system, a sonic orifice, and a crystal pressure transducer installed at the exit of the sampling tube. To obtain the enthalpy of a high temperature gas, a sample of the gas is aspirated through the sampling tube for a short time. The sampling tube has a large length-to-diameter ratio and is capable of absorbing most of the heat content of the flow sample. The sampling tube will steadily increase in average temperature. The rate of energy absorption in the tube can thus be inferred from rate of change of electrical resistance of the tube. Details of the probe and theory are well presented in Refs. 4 and 5. Photographs of the probe are shown in Figs. 6 and 7.

2.3.3 Stagnation Point Heat Transfer Probe

Several techniques are available for measuring local heat flux but most are limited to a heat transfer rate per unit area less than 1000 Btu/ft^2-sec. The presently accepted standard used to measure high heat transfer rates is the null-point calorimeter which is swept through the high enthalpy flow at high velocity. This gage requires a technique for manufacture which is proprietary to the Avco Corporation. Its design is based on the premise that there is a unique hole depth for a thermocouple below the heated surface at which the measured temperature is equal to the undisturbed surface temperature after a small time interval. If the surface temperature as a function of time is known, the heat flux can be calculated. This gage is well described in the literature and will not be discussed any further. Another gage, which measures surface temperature, is a coaxial thermocouple consisting of concentric Chromel® and constantan rods electrically insulated from each other. The thermocouple junction is made on the exposed surface by mechanical abrasion which smears the thermocouple material across the insulation gap, thus creating a thermocouple junction. This type of probe is very inexpensive and more readily available at AEDC than a null-point calorimeter. For these reasons, this type of gage was evaluated as a possible substitute for the null-point calorimeter gage. Both gages were installed in 0.25-in. nose radius models at the stagnation point.

2.3.4 Laser Shadowgraph

Flow visualization in high density arc facilities has for many years been limited to direct luminosity photographs. Conventional shadowgraph and schlieren techniques have not been feasible heretofore because of the intense radiation of light from stagnation regions in the flow. However, the special characteristics of a laser light source provide the possibility of the more conventional techniques because of: (1) narrow band emission which allows selective filtering of the hot gas emission, (2) high intensity to overpower this gas emission, and (3) high brightness to allow use of the high power without incurring the image-degrading properties of an extended source. The system used here contains a Q-switched laser to give instantaneous shadowgrams of the flow. A schematic of the system is shown in Ref. 4.

At best, the laser shadowgraphs shown in this report are fair. Through better optics and/or an aerodynamically quieter shroud flow, better photographs can be made so that details of shocks during ablation can be obtained.

2.3.5 Reentry Shape Models

Uncooled reentry shape models were tested to determine the pressure and heat transfer distributions on large models in the coaxial flow fields. The models designed for the test series were 0.50-in. radius, 0.25-in. radius, and a 0.50-in. radius spherical-nose models with a 10-deg half-angle conical afterbody (Fig. 8). (The 0.50-in. nose radius models were not actually tested because of time limitations.) Normally, models no larger than 0.25-in. nose radius are tested in arc-heated ablation facilities at this power level and hot flow diameter. The models were swept through the flow at a nominal 10 in./sec with no damage to the models. The pressure and heat transfer models had data collection points at the stations shown in Table I (Appendix II).

Pressures were measured by internally mounted piezoelectric crystal transducers close-coupled to each orifice. The pneumatic response of the systems was extremely good. The heat transfer distribution models contained null-point gages designed and installed by Avco. The test data were reduced to heat flux using the AROTHA program as described in Ref. 4.

To provide for evaluation of actual ablation testing in the cold shroud nozzle, a series of hemisphere-cylinder models were made of Teflon®. Nose radii of 0.25, 0.375, and 0.50 in. were provided.

SECTION III
RESULTS AND DISCUSSION

The performance of the cold shroud nozzle was evaluated by means of three different types of tests: flow field surveys, pressure and heat transfer distribution measurements on typical reentry shapes, and ablation tests. The parameters investigated were the length of the shroud extension, axial position of the model, the arc heater stagnation pressure level, the degree of matching of static pressures in the hot and cold flows, and model size. The optimum test configuration was determined principally by pressure measurements. The more complex and time-consuming measurements of heat transfer distribution and ablation rates were used mainly to provide a complete calibration of the optimum configuration and test conditions.

The addition of the cold shroud around the conventional hot jet nozzle had the purpose of elimination of the strong expansion at the exit of the hot jet nozzle and of the reduction of the flow disturbance emanating

from the nozzle lip to a negligible value. The purpose of the cold shroud extension was to allow a longer mixing length between the hot core flow and the cold shroud flow. The tests of Phase II had indicated that a beneficial effect at high arc heater pressure could be expected, by virtue of a reduced mixing layer thickness. There was also evidence in the Phase II testing that a slight mismatch in the hot and cold jet static pressures could in some cases produce small beneficial changes in pressure distribution observed on large models.

3.1 COAXIAL FLOW FIELD SURVEYS

The flow fields produced by the cold shroud nozzle were surveyed with the boundary layer probe, the two stagnation point heat transfer probes, and with the transient enthalpy probe. The nominal values of the arc heater and nozzle operating parameters which were used for these surveys are listed in Table II. The range of arc heater pressures of 20 to 80 atm was covered with matched static pressures in the hot and cold flows. At 60 atm arc heater pressure, a range of static pressure ratios across the mixing region of 0.75 to 1.34 was covered. It was not anticipated that extremely high stagnation enthalpy levels would be necessary to evaluate the capability of the cold shroud nozzle, hence a nominal value of 2000 Btu/lbm was used, which was entirely adequate for the ablation measurements on the Teflon models.

3.1.1 Pitot Pressure Profiles

The cold flow pitot pressure profiles in Fig. 9 were obtained at various probe injection speeds to establish that the pressure probe response characteristics were adequate to follow the pressure changes through the mixing zone and across the local shock waves generated in this mismatched flow. The shadowgram in Fig. 10 is representative of the shock patterns in the cold jet. As a reference, the outer cold flow nozzle diameter is 1.6 in., and the inner flow nozzle diameter is 0.70 in.

The pitot pressure profiles measured for the hot flow test conditions of Table II are presented in Figs. 11, 12, and 13 for shroud extensions of 0, 0.8, and 1.6 in., respectively. The profiles have been normalized by the local stagnation pressure at the centerline of the hot flow in order to provide a direct comparison of the effect of different pressure levels on the mixing zone. (At the $x/r_e = 0.5$ station probed downstream of each shroud extension, this pressure is approximately 0.41 of the arc heater total pressure.) There are two parts to each of Figs. 11 to 13: a series of profiles with matched static pressures covering the complete range of arc heater pressure and, for a heater pressure of 60 atm,

three profiles are presented for three different ratios of static pressure across the hot-cold mixing layer.

In Fig. 11, the pitot pressure profiles obtained with no shroud extension demonstrate that the arc heater pressure has no effect on the width or the depth of the mixing region for the range of pressures from 20 to 80 atm (nominal). Even though it was attempted to obtain a condition of matched static pressures, a significant shock compression is seen to exist in the hot flow at the edge of the mixing region. It is believed that this wave results from the physical disturbance at the end of the hot core nozzle, represented by the finite lip thickness and a nonzero wall angle. This wave can be intensified or converted to an expansion wave by changing the cold shroud pressure, as shown in the upper part of Fig. 11.

In Figs. 12 and 13, it can be observed that the use of a cold shroud extension has the net effect of smoothing the hot core flow at the expense of increased shock systems in the cold shroud flow. In addition, of course, the increased length of flow results in a widening of the mixing region. The minimum stagnation pressure in the mixing zone, however, does not vary much with the length of extension. As the shroud extension length is increased, the influence of the shroud pressure on the hot flow is decreased.

It appears that the benefit of the shroud extension is to move the final expansion wave disturbance well downstream of the exit of the hot core nozzle, which permits testing to be done in the hot core at a position sufficiently far downstream to clear the lip shock from the hot core nozzle, which crosses the mixing zone and leaves only a weak reflection from the mixing layer in the hot core flow. The disturbances at the hot nozzle exit are visible in the photographs of the high enthalpy flow without the shroud extension (Fig. 14). These disturbances are not visible when either of the two extensions are used, which appears to verify that the lip shock has been greatly weakened at axial locations corresponding to the exit of the two extensions.

At axial locations far downstream of the 1.60-in. extension (Fig. 15), the overall flow widens and the mixing zone widens to such an extent that the hot core is no longer useful.

The variation of the centerline stagnation pressure downstream of each of the three shroud extension configurations is presented in Fig. 16, normalized by the arc heater stagnation pressure. The variation is very nearly the same for all three cases. Although the exit of the 1.6-in. shroud extension is located physically in the second rhombus of the hot

core nozzle, there is no reduction in stagnation pressure at this point, compared with the exit of the hot core nozzle with no shroud extension.

3.1.2 Stagnation Point Heat Transfer Profiles

The character of the hot core flow field at the exit of the 1.60-in. shroud extension was further defined by measuring stagnation point heat transfer profiles at $x/r_e = 0.50$ (Figs. 17 to 20) for arc heater pressures of 20 to 80 atm. These data were obtained with the coaxial heat flux probe and with a null-point calorimeter probe. The heat transfer rates were calculated from the rates of increase of probe temperature by means of the AROTHA computer program, as noted in Ref. 4. The total enthalpy data presented in Figs. 17 to 20 were inferred from the heat transfer rates by assuming a laminar boundary layer on the probes and the following relation between heat flux and total enthalpy:

$$H_o = \frac{\dot{q}_{HW}}{0.133} \frac{R_N}{p_o'} + H_{o_{HW}}$$

which is an approximation based on the well-known Fay-Riddell relation for stagnation point heat transfer in laminar flow.*

When a comparison is possible, the results from both probes are in reasonably good agreement. Both probes indicate a large increase in heating rate in the vicinity of the mixing zone between the hot and cold flows. Although the inferred enthalpy profiles exhibit the same behavior, it does not appear to be realistic to ascribe the heat flux increases to stagnation enthalpy peaks, since the measured enthalpy profiles do not evidence any such shapes, Section 3.1.3. Rather, the measured heat transfer peak is believed to be the result of turbulent heat transfer in and near the mixing zone.

In Fig. 21, the measured stagnation pressure and heat transfer profiles for the 20-atm case are compared with calculations based on the turbulent mixing theory (Ref. 6). The measured pitot pressure profile and the measured stagnation enthalpy obtained with the enthalpy probe are in reasonable agreement with the theoretical profiles, which is a strong indication of a turbulent mixing zone. The peaks in the enthalpy profiles inferred from stagnation point heating rates are thus suggested to be anomalies resulting from the use of the (laminar) Fay-Riddell theory in making the inference.

---

*This approximation was developed by use of a representative viscosity for air and a Newtonian pressure distribution.

3.1.3 Stagnation Enthalpy Profiles

In addition to the inferences of stagnation enthalpy discussed in the previous section, stagnation enthalpy profiles at the exit of the cold shroud nozzle were measured by the transient enthalpy probe. This probe is considered to be in the developmental stage and there exist reservations as to the accuracy of the absolute values of enthalpy measured by it. (The response of the probe is subject to influences of heat loss and nonlinear resistivity which have not yet been fully analyzed, Ref. 4.) Even at this stage of development, however, it is believed the general shapes of measured enthalpy profiles are reasonably valid.

In Fig. 22 are presented unsmoothed data obtained by traverses of the enthalpy probe in opposite direction across the hot jet flows for heater pressures from 20 to 80 atm. The large indicated oscillations of enthalpy are the result of electrical noise in the rapid-scan analog-to-digital converter system used with the transient probe. The average enthalpy values are in all cases less than values given by a heat balance on the arc heater. When an average profile is obtained by fairing through the oscillations produced by the digital readout, it is apparent that no local increase in total enthalpy is present near the mixing zone, as indicated in the inferred enthalpy data in Figs. 17 to 20.

A summary of stagnation enthalpy data obtained from five different sources is presented in Table III. The average probe enthalpy varied from 0.647 to 0.99 of the heat balance enthalpy, but this is appreciably closer to the heat balance values than are the enthalpies inferred from the heat transfer measurements.

3.2 REENTRY-SHAPE MODEL TESTS

Testing of the reentry-shape models was planned to demonstrate the capability of the cold shroud nozzle to produce valid flows over models which are appreciably larger than the diameter of the hot core flow. Since a 0.25-in. nose radius model is usually considered a limiting size for a conventional hot jet of the same size as used in the present study, a 0.50-in. nose radius model was selected for evaluation in the cold shroud nozzle. It was assumed that the 0.25-in. nose radius model could be tested in the cold shroud nozzle with only minor differences in flow compared with an unshrouded hot nozzle. In view of the size of the larger model in relation to the hot core diameter, it was desired to determine whether any major differences in flow pattern would occur. In addition, it was desired to study in some detail the minor effects on the model flow of shroud extension length, model

position, arc heater pressure, and degree of matching of the hot and cold flow static pressures. That minor effects would be present is clear from examination of Fig. 23, which shows some of the flow field features as derived from stream measurements and shadowgrams. The hot jet has an internal field of weak disturbance waves which means there should be an optimum position for a model to be tested. For no shroud extension and for the 0.8-in. extension, a fairly strong lip shock is present at the nozzle exit. With the 1.6-in. extension, however, the lip shock has crossed into the cold shroud flow upstream of the exit, leaving only a weak reflected wave in the core. The shadowgraphs are for cold flows, but they appear to be good approximations to hot flow.

Testing was performed at four axial positions downstream of the three shroud configurations, with four arc heater pressures between 20 to 80 atm, with three conditions of static pressure ratio across the hot jet and cold jet boundary, and with two model sizes. It was obviously not practical to test all possible combinations of these variables, nor is it even convenient to present results from all of those which were tested. Only a selection of the more important results will be presented.

3.2.1 Pressure Distributions

The pressure distributions on the sphere-cone models were obtained by reading all of the model pressures at the instant the model was at the centerline of the hot core flow. These distributions normalized by the stagnation point pressure on the model and averaged over two complete sweeps of the model are given in Figs. 25 to 28 for the 0.5-in. nose radius model and in Fig. 29 for the 0.25-in. nose radius model. Only a limited amount of testing was done with the smaller model since there was no real fundamental question of suitability of that model in the 0.7-in. hot flow. The theoretical pressure distributions were calculated by the method of Ref. 7. The M = 2.5 case was chosen to correspond to the design Mach number of the hot core flow and the M = 10 case was chosen to correspond more nearly to a representative flight condition.

A simple demonstration of the advantage gained by use of a cold shroud is represented by the pressure distributions obtained on the 0.50-in. nose radius model immersed in the flow of the inner jet only (cold) and in the combined flow of the inner and outer jets (Fig. 24). (This test could not be performed with a hot core flow because the cold shroud flow is required for adequate cooling of the hot core nozzle when operating with the arc heater.) The impingement of the 0.7-in.-diam

flow on the 1-in. -diam nose produces a pressure distribution which is close to the M = 10 theory up to 45 deg from the stagnation point, but which falls rapidly to ambient pressure beyond this point. As a result, part of the spherical nose is at an underpressure condition and the pressure on the conical section is higher than either of the two theoretical curves. Addition of the cold shroud flow restores the pressure distribution on the nose to values representative of the M = 10 theory, but on the conical surface, the pressures are even higher than for the unshrouded case.

Repeatability of the pressure distribution measurements made in the hot shrouded flow is demonstrated in Fig. 25, for a heater pressure of 20 atm and 0.80-in. shroud extension. This combination of operating parameters is not necessarily optimum, thus a comparison of the experimental data with the theoretical curves is not especially important. Nevertheless, it is noted that the agreement is better with the M = 10 calculation upstream of the tangency point and with the M = 2.5 calculation downstream of the tangency point. This appears to be the result of an inadequate pressure ratio, at 20-atm arc heater pressure, to sustain the proper expansion of flow over the conical surface.

The effect of the model axial position with respect to the flow exit, x/r_e, is presented in Fig. 26, for a heater pressure of 80 atm, no shroud extension, and matched static pressures. These data show reasonable agreement with the M = 10 theory for an x/r_e = 1.0 and nearly as good agreement at x/r_e = 0.5. However, for x/r_e greater than 1.0, over-expansion of the flow around the sphere-cone junction due to enlarging of the mixing zone in the free jet expansion is observed. In addition, testing at large x/r_e results in a rather drastic reduction in model stagnation pressure (Fig. 16). Because of the resulting decrease in heat flux, it is important in ablation testing to maintain the model at small values of x/r_e.

The effects of arc heater pressure and degree of matching of static pressures in the hot and cold flows are presented in Figs. 27a and b for x/r_e = 1.0 with the 0.8-in. shroud extension. The pressure distributions with matched static pressures (Fig. 27a) exhibit at all heater pressures a marked "dip" in the vicinity of the 45-deg station on the spherical nose. This location is very close to the point of intersection of the extended mxing zone with the spherical nose. Otherwise, the agreement of experiment and theory is better with the M = 10 curve on the nose of the model, but intermediate to the M = 2.5 and M = 10.0 curves on the conical surface. There is some evidence of approach to the M = 10 curves as the arc heater pressure is increased. By variation of the degree of matching of static pressures in the hot and cold

flows, some measure of control over small details in the pressure distribution, such as the dip noted in Fig. 27a, can be obtained. In Fig. 27b, it is seen that a cold shroud overpressure of about 22 percent results in a near disappearance of the dip in the distribution on the nose of the model, but at the expense of an overpressure farther downstream. Decreasing the shroud pressure below the matched condition is observed to accentuate the dip in the pressure distribution, with only a minor effect on the distribution on the conical part of the model.

The effects of heater pressure and degree of static pressure matching with the 1.6-in. shroud extension are presented in Figs. 28a and b. At this distance downstream of the lip of the hot core nozzle, the wave patterns inside the hot core are such as to reduce the magnitude of the dip in the pressure distribution at the 45-deg location to a value considerably less than found with the shorter extension (Fig. 28a). As a result, acceptable agreement of experiment and theory is found for all heater pressures except the lowest (20 atm). The M = 10 simulation is quite good at the theoretical intersection of the mixing zone and the spherical nose and very close to M = 10 on the conical surface. Changing the shroud pressure (Fig. 28b) resulted in only minor changes in pressure distribution except at the 22.5-deg station. These changes are presumed to be a result of relocation of minor shock waves in the core flow caused by the different pressure field.

The smaller nose radius model (0.25-in.) was tested for the purpose of determining if the cold shroud would allow valid afterbody measurements to be made at large values of S/R_N. These data are presented in Fig. 29 for a heater pressure of 80 atm, a 1.6-in. shroud extension, matched pressures, and at $x/r_e = 1.0$. The distribution of pressure transducers on the spherical tip of this model is quite sparse, but the test data appear to agree better with the M = 10 calculation on the spherical nose. On the conical afterbody, good agreement with the M = 2.5 calculation is observed for S/R_N up to 4.4.

3.2.2 Heat Transfer

The large (0.50-in.), five-channel heat transfer model was swept through the flow at an arc heater pressure of 80 atm. Figure 30 presents the heat transfer rate distribution with no shroud extension, 0.80-in. extension, and 1.6-in. extension. When the model is tested close to the hot nozzle exit (that is, no extension), the interaction with the lip shock causes a large degree of heating on the model near the sonic point and slightly beyond. With the 0.80-in. extension, the overheating is still present but is reduced in magnitude by a factor of one-half. The distribution obtained with the 1.6-in. extension shows

excellent agreement with the theoretical distribution, and only minor deviations are apparent. The heat flux at the stagnation point for the data shown in this figure is about 3450 Btu/ft^2-sec.

The smaller 0.25-in. radius heat transfer model was tested at an arc heater stagnation pressure of 80 atm. Figure 31 shows the heat transfer distributions with the three shroud extension configurations. It was unfortunate that the heat transfer gage at an S/R of 2.0 was bad, since this would have given a little more confidence in the shape of the experimental distributions. As with the larger model, the longer shrouds force the data closer to the theoretical curve on the hemisphere portion of the body, but in general, the agreement with theory is not as good as with the larger model.

3.3 ABLATION MODEL TESTS

A number of runs were made with Teflon hemisphere-cylinder models having nose radii of 0.25, 0.375, and 0.50 in. to determine if large reentry-type models could be ablated uniformly with the shrouded flow. Figures 32 to 35 show some of the results of this study which were performed with the 1.6-in. shroud extension. Each ablated model shown in the photographs is typical of the three models ablated at each condition. A literature search failed to disclose any information on the changes in shape experienced by Teflon samples in standard ablation facilities; therefore, "standard" data were generated in the AEDC Arc Heater Test Unit (5 MW), a User-test facility which operates at higher pressures than does the 5-MW Research Arc Heater. Teflon ablation models were tested in this facility using a conventional M = 2.0 nozzle (r_e = 0.255) and no cold shroud. Ablation rate data and profile changes were obtained at model pressures up to 80 atm. Figure 36 shows the profiles obtained during ablation of the models in the cold shroud facility as well as some of the profiles obtained with the 5-MW standard nozzle. The small 0.25-in. nose radius models result in similar profiles from both facilities showing that the cold shroud does not adversely affect the flow from small nozzle-model combinations. The large 0.50-in. nose radius models tested in the cold shroud facility resulted in shape changes very much like the small model proving the validity of the technique. However, similar tests on the large model in the standard nozzle of the 5-MW ablation facility definitely show a concave ablation pattern. Since this is a three-dimensional effect, once the concave profile is reached, the ablation is hidden by the outer rim, and it is nearly impossible to measure accurately the ablation rate. This result is typical for a model which is too large for the available flow. It is not surprising that the large model ablated

properly and uniformly in the cold shroud facility and poorly in the non-shrouded facility since the shrouded flow supplies the proper heat transfer and pressure distributions around the model when operated in the optimum configuration (Refs. 1, 2, and present data). The recession of the model surface with time for the ablation tests in the cold shroud nozzle are given in Fig. 37. Excellent repeatability for each model size tested can be observed. The time zero point was chosen to coincide with the time ablation appeared to begin, after which the nose tip receded linearly for a considerable time. Eventually, however, nonlinear increase in recession rate is observed.

In order to compare these recession data with other facilities and to provide a theory for comparison, Eq. (8) of Ref. 9 was used. This equation takes the form:

$$\dot{m} = \frac{0.0046\,(p_o')^{0.24}\,(\dot{q}_{cw})^{0.55}}{(R_N)^{0.21}}$$

Comparisons of the measured recession rates in the cold shroud nozzle with predictions of this equation are given in Fig. 38. The predicted recession rate was calculated first using the average (heat balance) enthalpy of the arc heater, and a second calculation was made using the cold wall heat flux data from the heat transfer models. Agreement between the recession rate calculated using the heat transfer model data and the measured recession rate is excellent. The measured data were taken during the first half second of ablation.

Finally, the Teflon ablation rate data obtained with the cold shroud nozzle, using measured heat flux data for data reduction, are compared in Fig. 39 with the above equation with test data from other ablation facilities reported in Ref. 9, and with the Teflon ablation rate data measured in the AEDC Arc Heater Test Unit (5 MW). The cold shroud nozzle data agree with the correlation curve as well as the data from any other source.

SECTION IV
CONCLUDING REMARKS

This phase of testing confirms most of the results reported for the Phase I and II tests and has extended the calibration of the cold shroud nozzle. The use of transient instrumentation techniques has made the calibration of these facilities much easier and more comprehensive.

The shroud technique provides a hot jet which results in excellent data agreement with theoretical pressure and heat transfer distributions for models considerably larger than the hot jet. Ablation data for both small and large models show proper ablation profiles and recession rates which correlate with all other arc facilities.

The technique provides the proper aerothermodynamic flow simulation about very large reentry-type models. The size models which can be tested in this 5-MW cold shroud facility are several times larger than those normally tested in any existing facilities at comparable test conditions. Because large jet size can be simulated with an order of magnitude less power, many of the inherent problems of the higher power facilities can be avoided without sacrificing model size and simulation. Alternatively, larger size facilities can be built with much reduced power and therefore cost. There is no indication that the shroud size chosen for this study is optimum. In fact, it is anticipated that the effective size of a facility may be increased considerably by utilizing a larger cold shroud.

REFERENCES

1. Herron, R. D. "Ablation Testing in Hot and Cold Coaxial Jets – Phase I, Cold Flow Feasibility Tests." AEDC-TR-70-64 (AD704545), April 1970.

2. Herron, R. D. "Ablation Testing in Hot and Cold Coaxial Jets." AIAA paper No. 70-588, May 1970.

3. Baker, W. B., Jr. and High, M. D. "Measurement of Enthalpy Distribution at the Exit of a 5-MW Arc Heater as Obtained by an Ablation Technique." AEDC-TR-69-212 (AD697769), November 1969.

4. Pigott, J. C., Smith, R. T., and MacDermott, W. N. "Development of Calibration Instrumentation for Ablation Facilities." AEDC-TR-71-172, September 1971.

5. Vassallo, F. A. "Miniature Enthalpy Probes for High Temperature Gas Streams." ARL66-0115, June 1966.

6. Patankar, S. V. "Heat and Mass Transfer in Turbulent Boundary Layer." PhD Thesis, Imperial College of Science and Technology, University of London, June 1967.

7. Weilerstein, Gertrude. "The Addition of Secondary Shock Capability and Modifications to the GASL Three-Dimensional Characteristics Program. Part II. User's and Programmer's Manual." GASL TR-653 (AD666742), August 1967.

8. Winovich, Warren. "On the Equilibrium Sonic-Flow Method for Evaluating Electric-Arc Air-Heater Performance." NASA TN D-2132, March 1964.

9. Hiester, N. K. and Clark, C. F. "Comparative Evaluation of Ablating Materials in Arc Plasma Jets." NASA CR-1207, December 1968.

APPENDIXES

I. ILLUSTRATIONS

II. TABLES

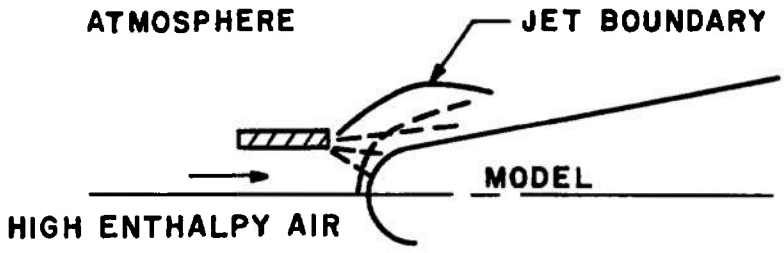

a. Present Testing Technique

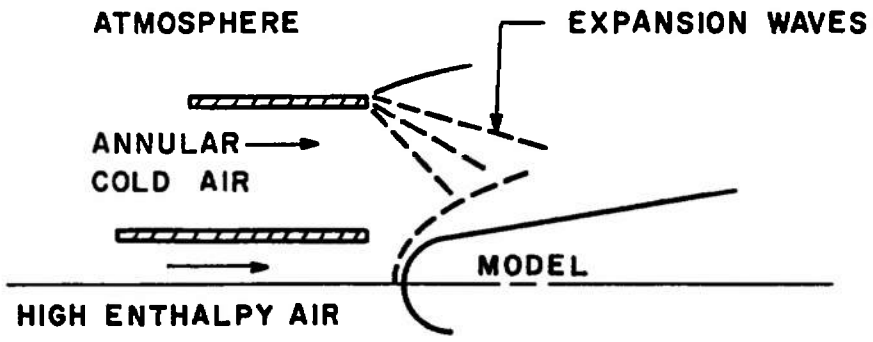

b. Coaxial Flow Testing Technique

Fig. 1 Application of the Coaxial Flow Technique to Ablation Testing

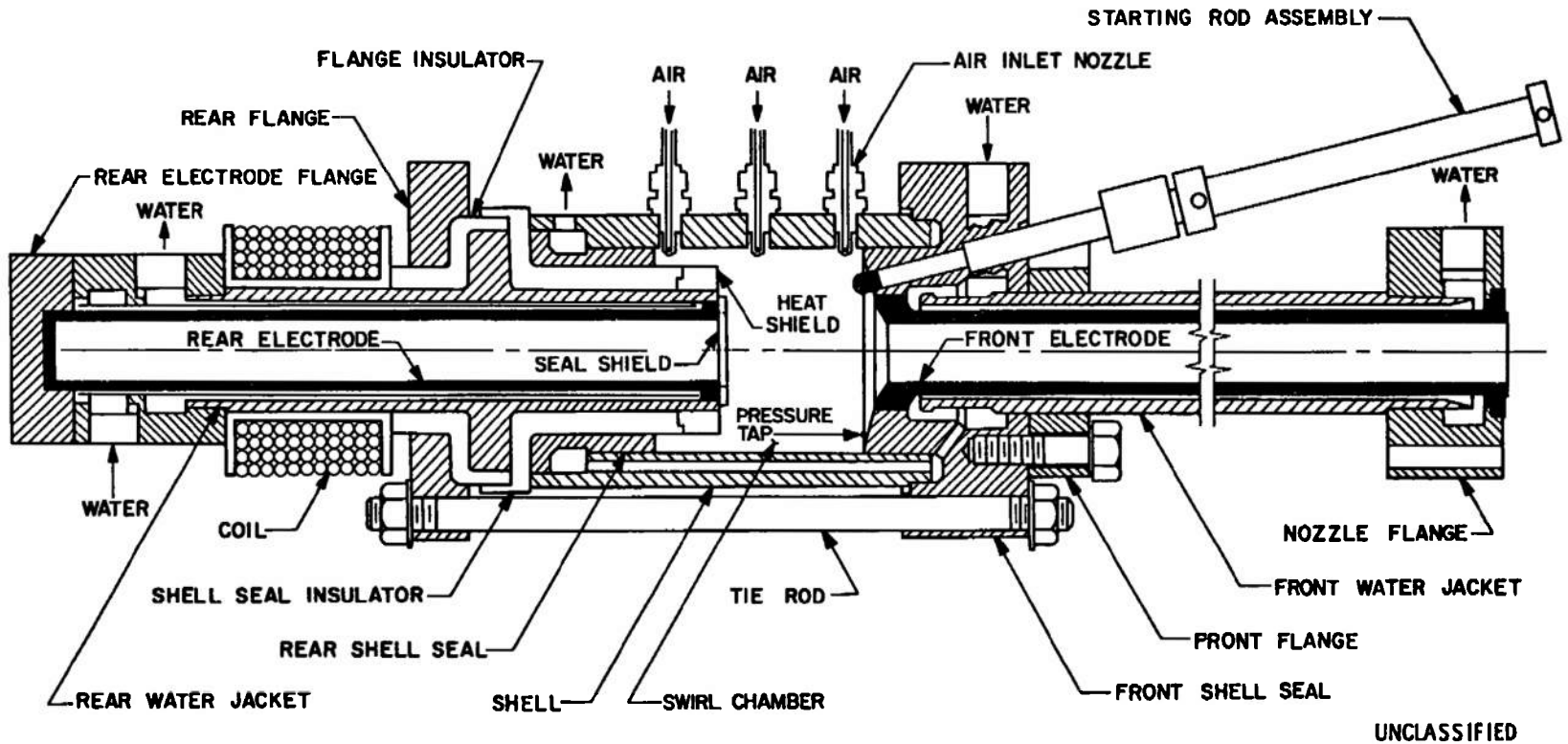

Fig. 2 Section View of Research Arc Heater

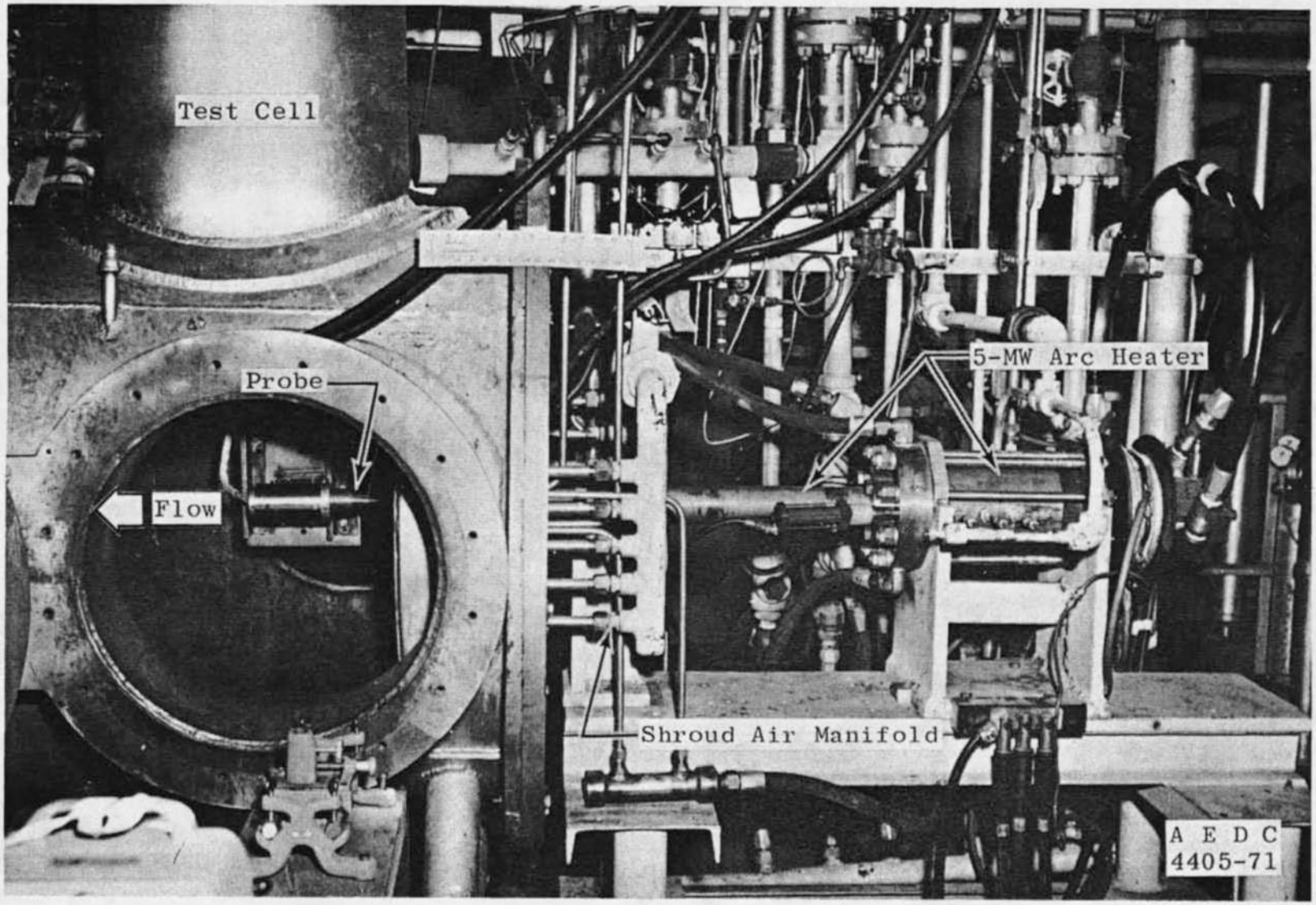

Fig. 3 Research Arc Heater Test Cell

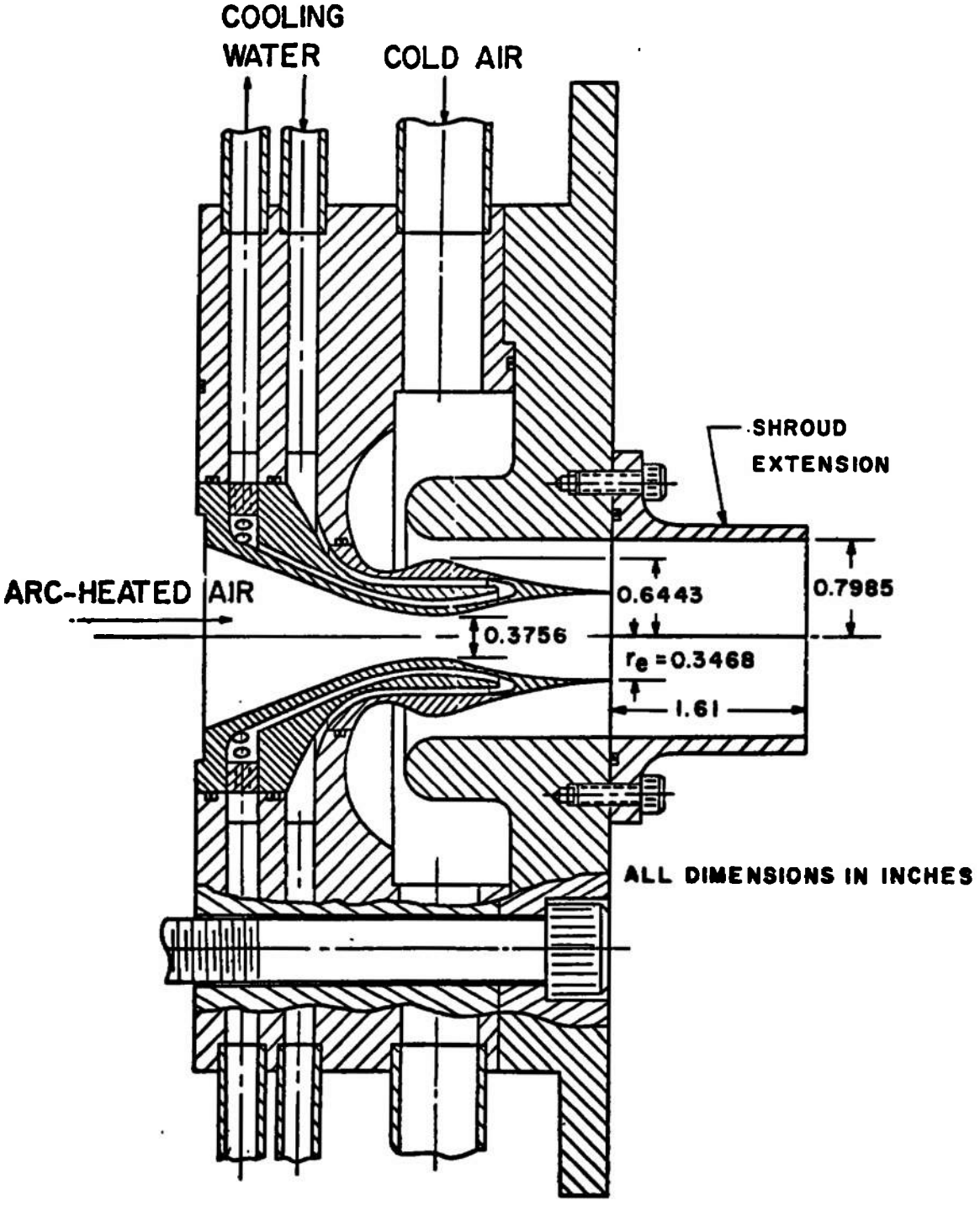

Fig. 4 Coaxial Flow Nozzle Assembly

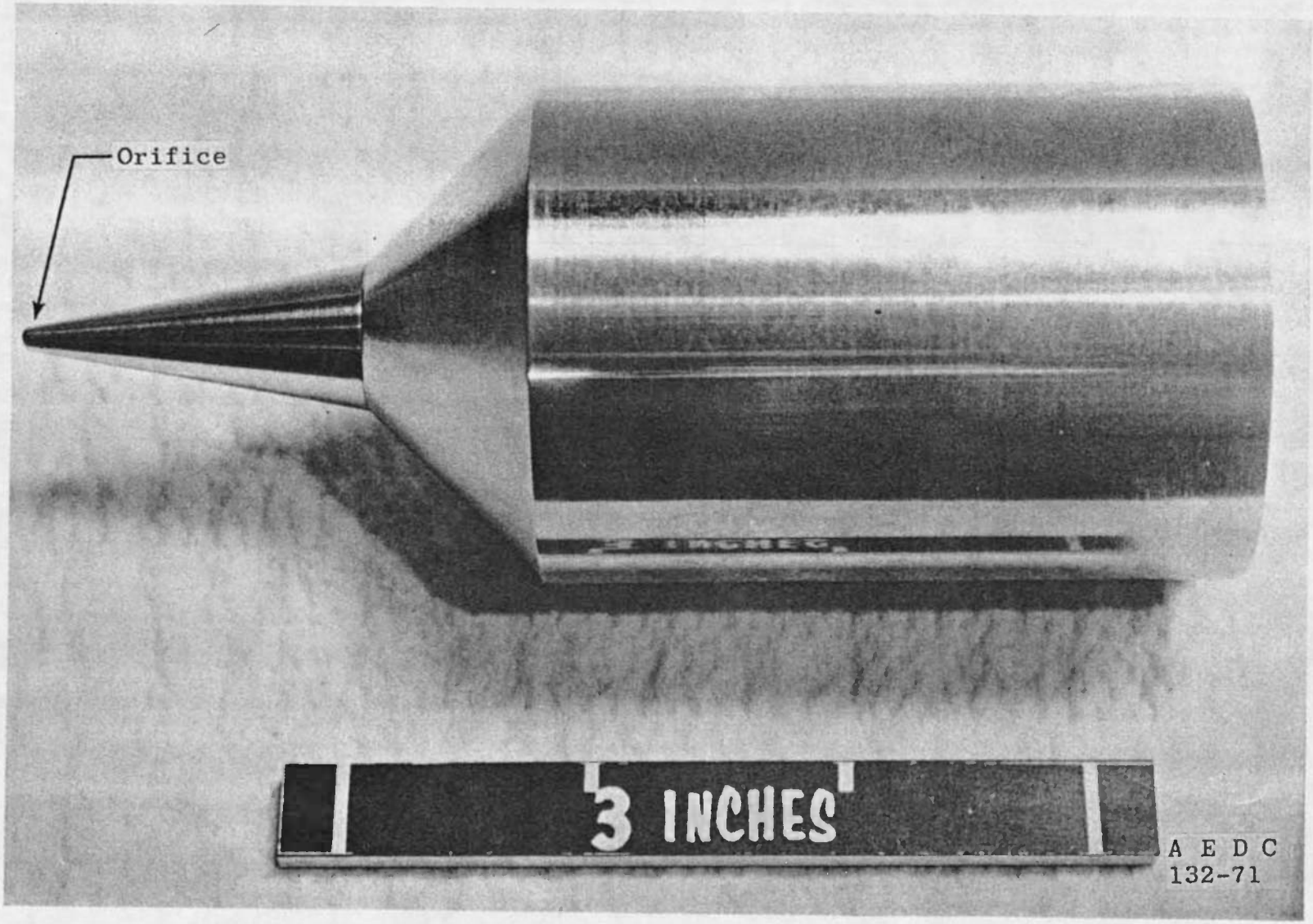

Fig. 5 Transient Boundary Layer Probe

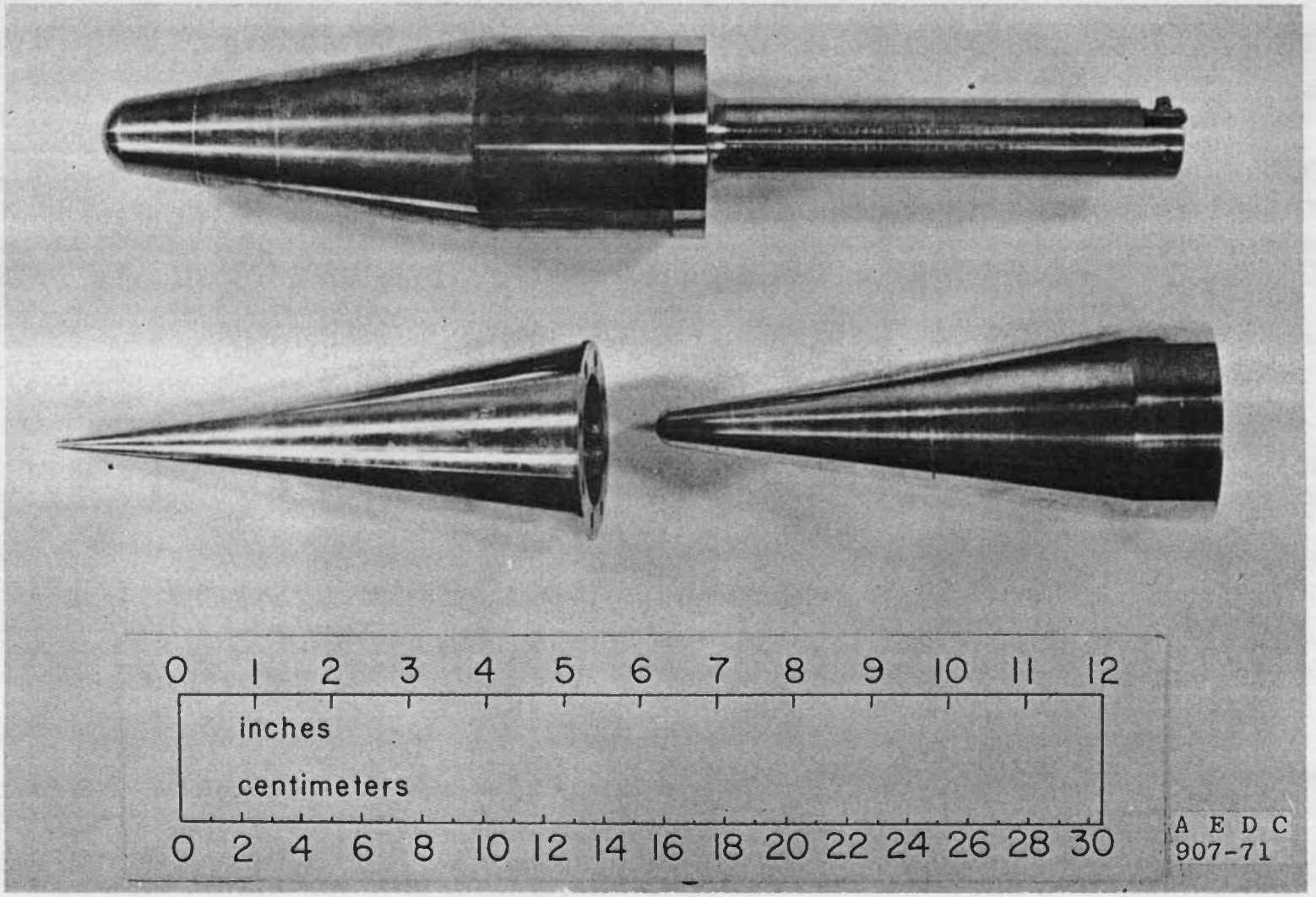

Fig. 8 Reentry Shape Models

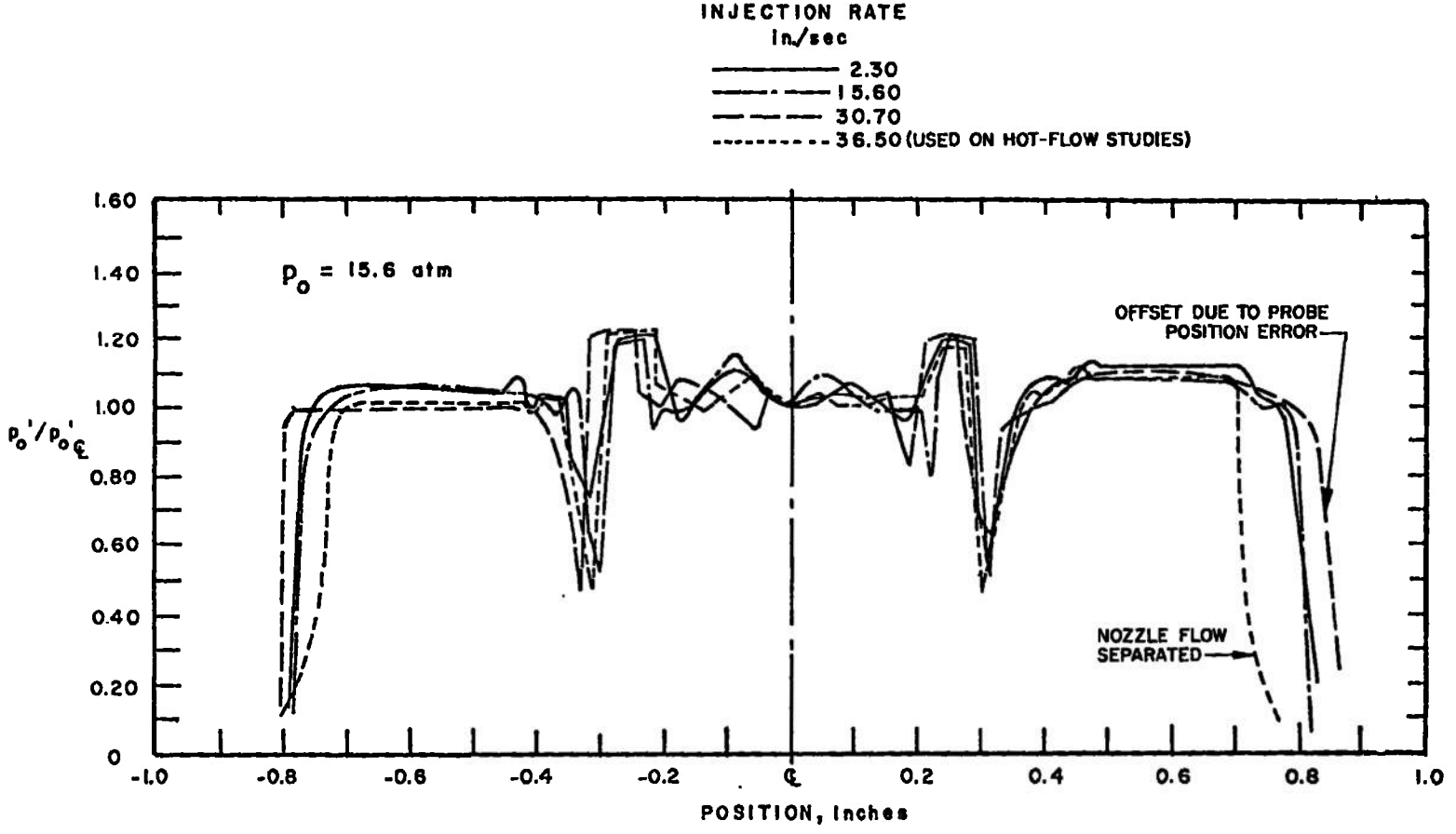

Fig. 9 Cold Flow Pitot Pressure Distributions Showing Pressure Response

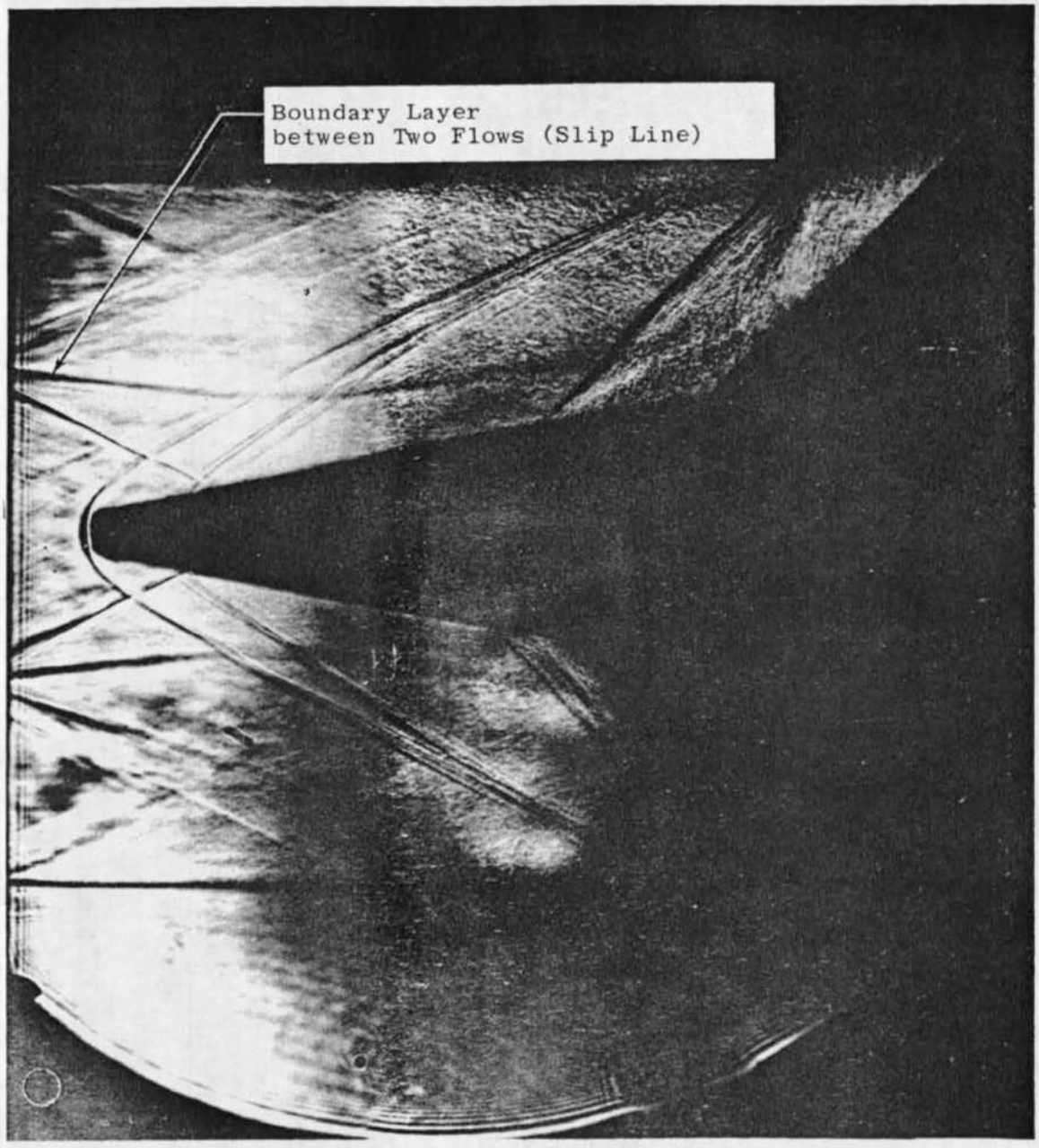

Fig. 10 Cold Flow Shadowgram of Transient Boundary Layer Probe

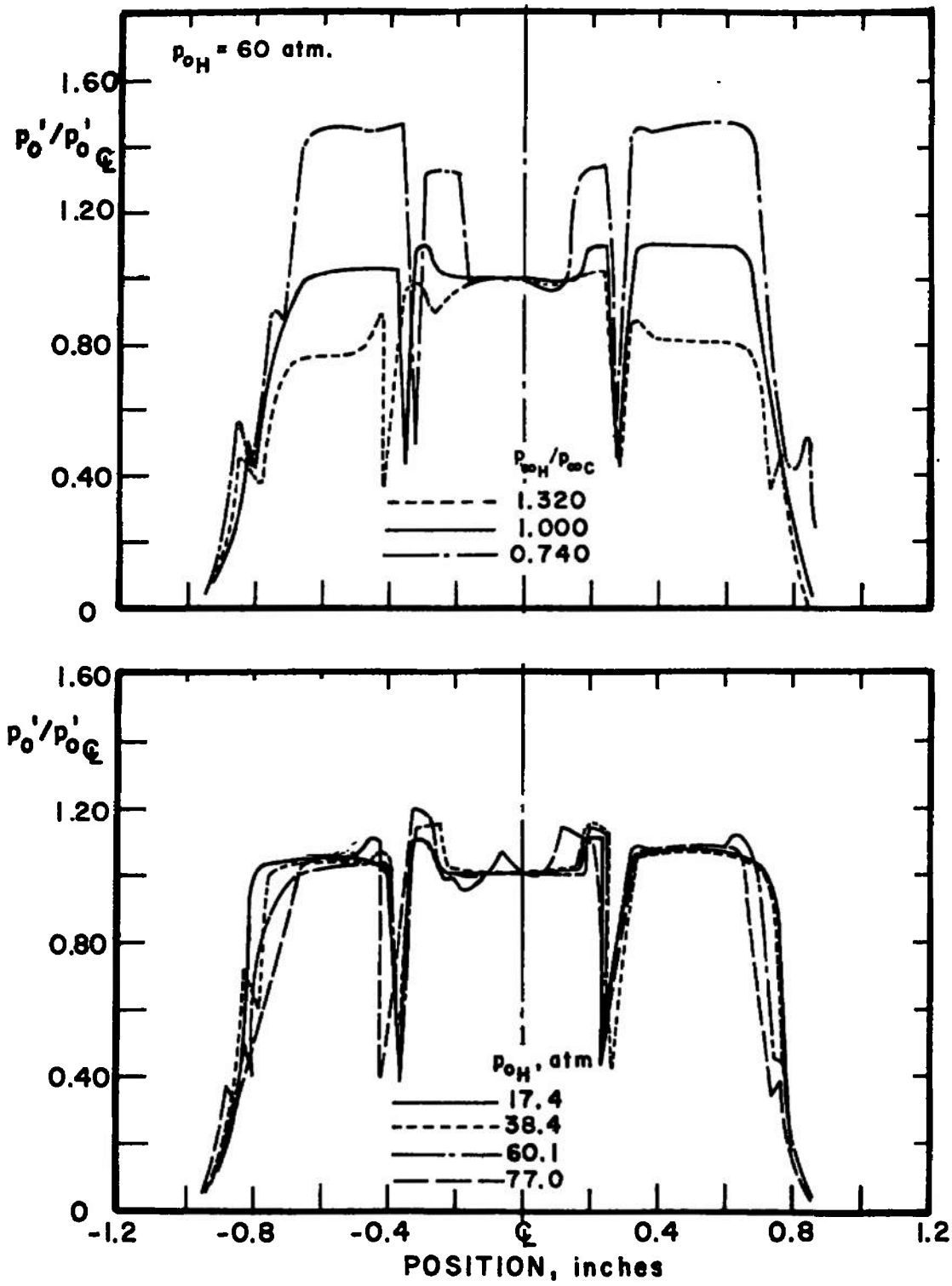

Fig. 11 Pitot Pressure Profiles of Coaxial Flow Fields, No Shroud Extension

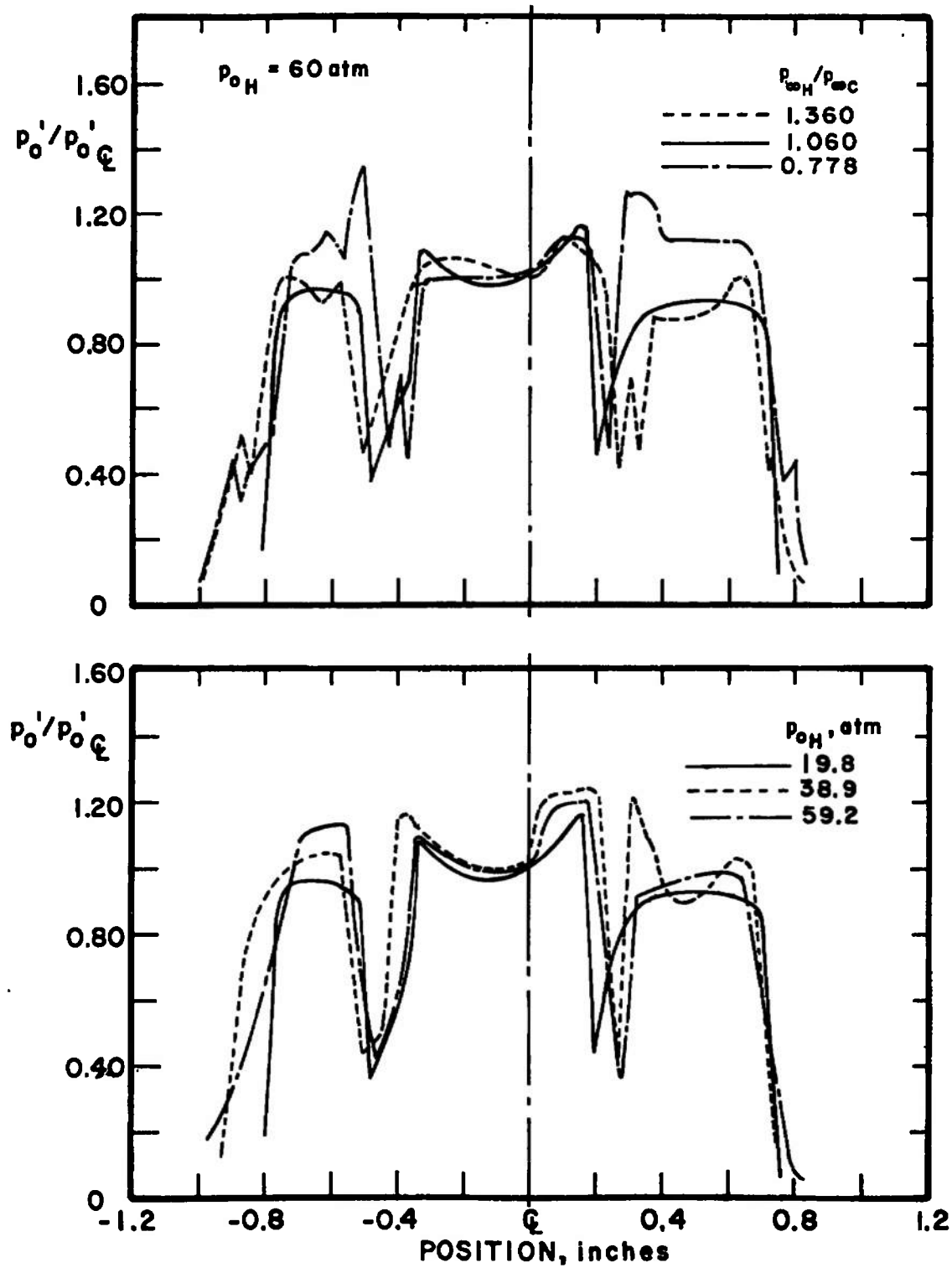

Fig. 12 Pitot Pressure Profiles of Coaxial Flow Fields, 0.80-in. Shroud Extension

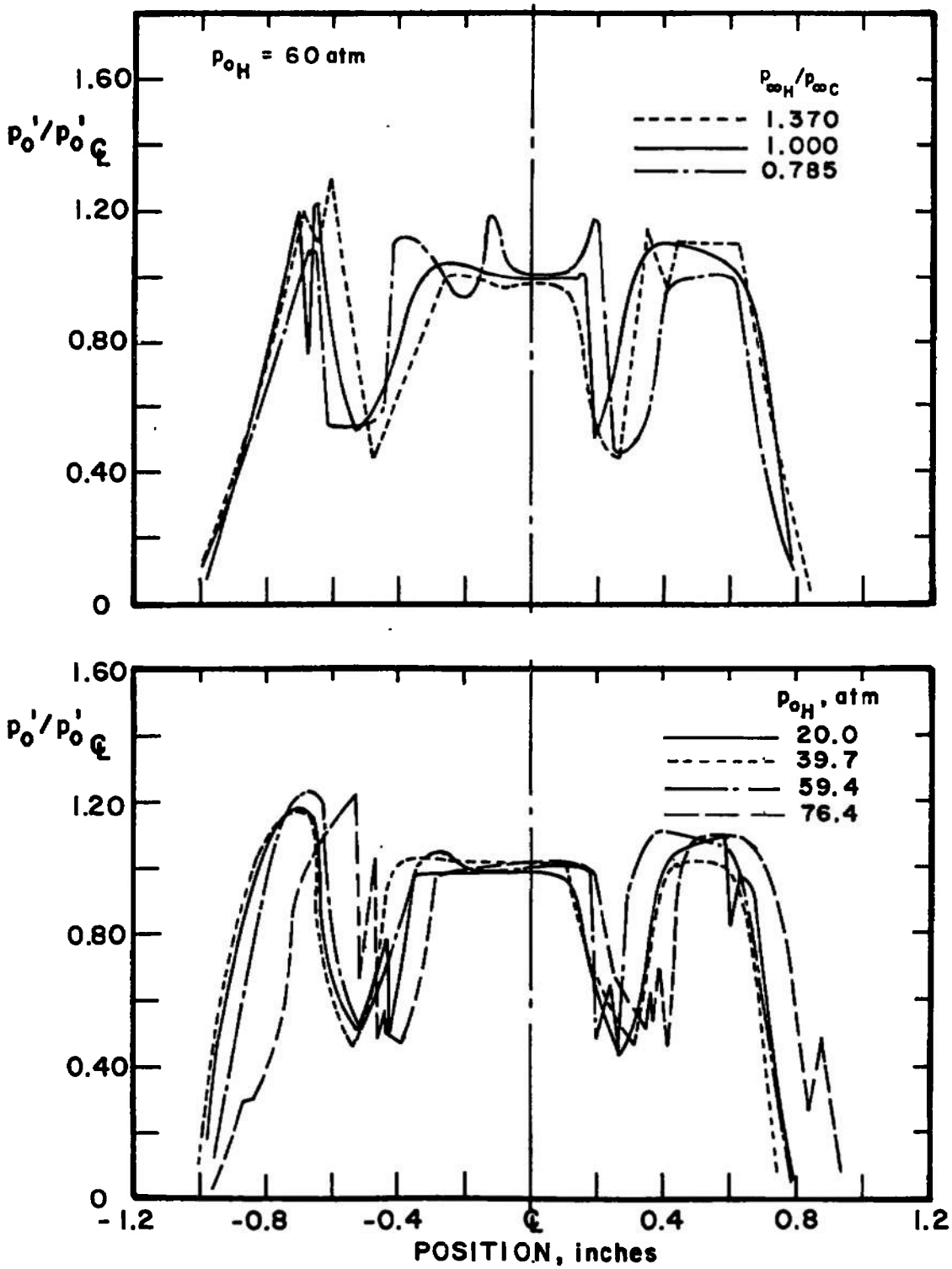

Fig. 13 Pitot Pressure Profiles of Coaxial Flow Fields, 1.60-in. Shroud Extension

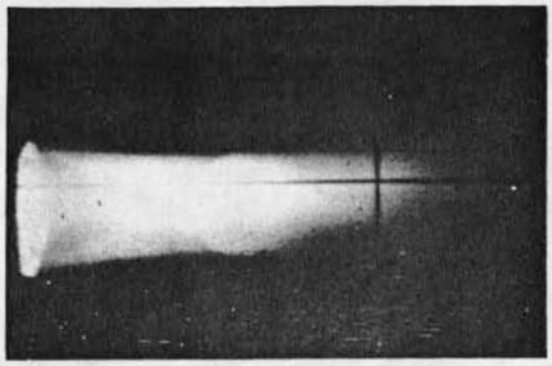

NO SHROUD EXTENSION

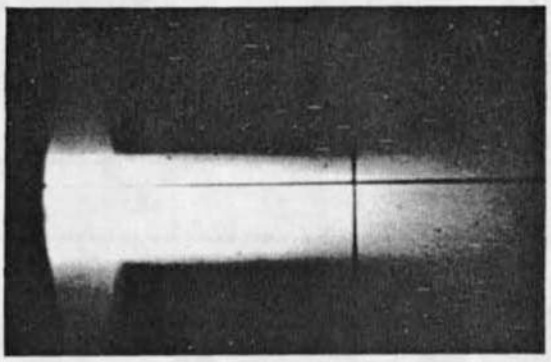

0.80 INCH SHROUD EXTENSION

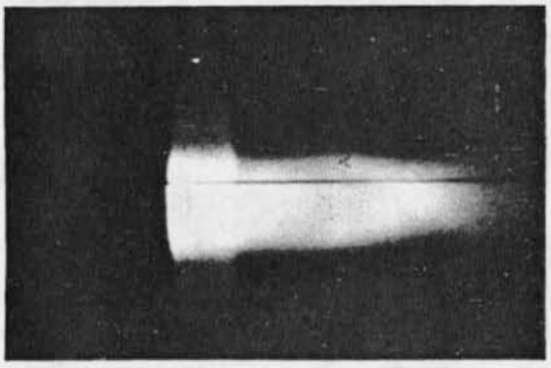

1.60 INCH SHROUD EXTENSION

Fig. 14 Photographs of the Flow from the Shrouded Nozzle at Arc Heater Stagnation Pressure of 80 atm

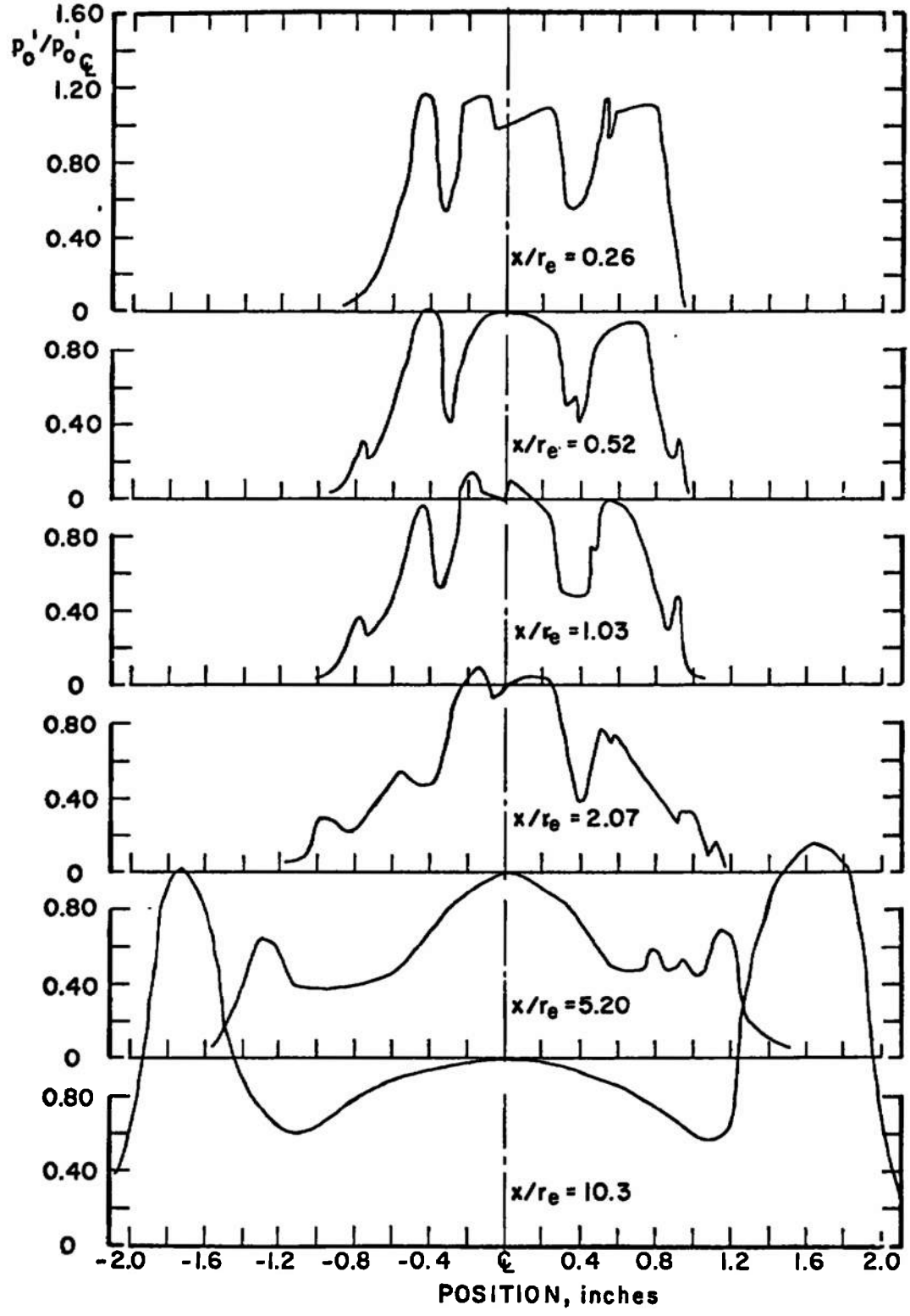

Fig. 15 Pitot Pressure Distributions at Various Axial Stations Downstream of the 1.60-in. Shroud Extension

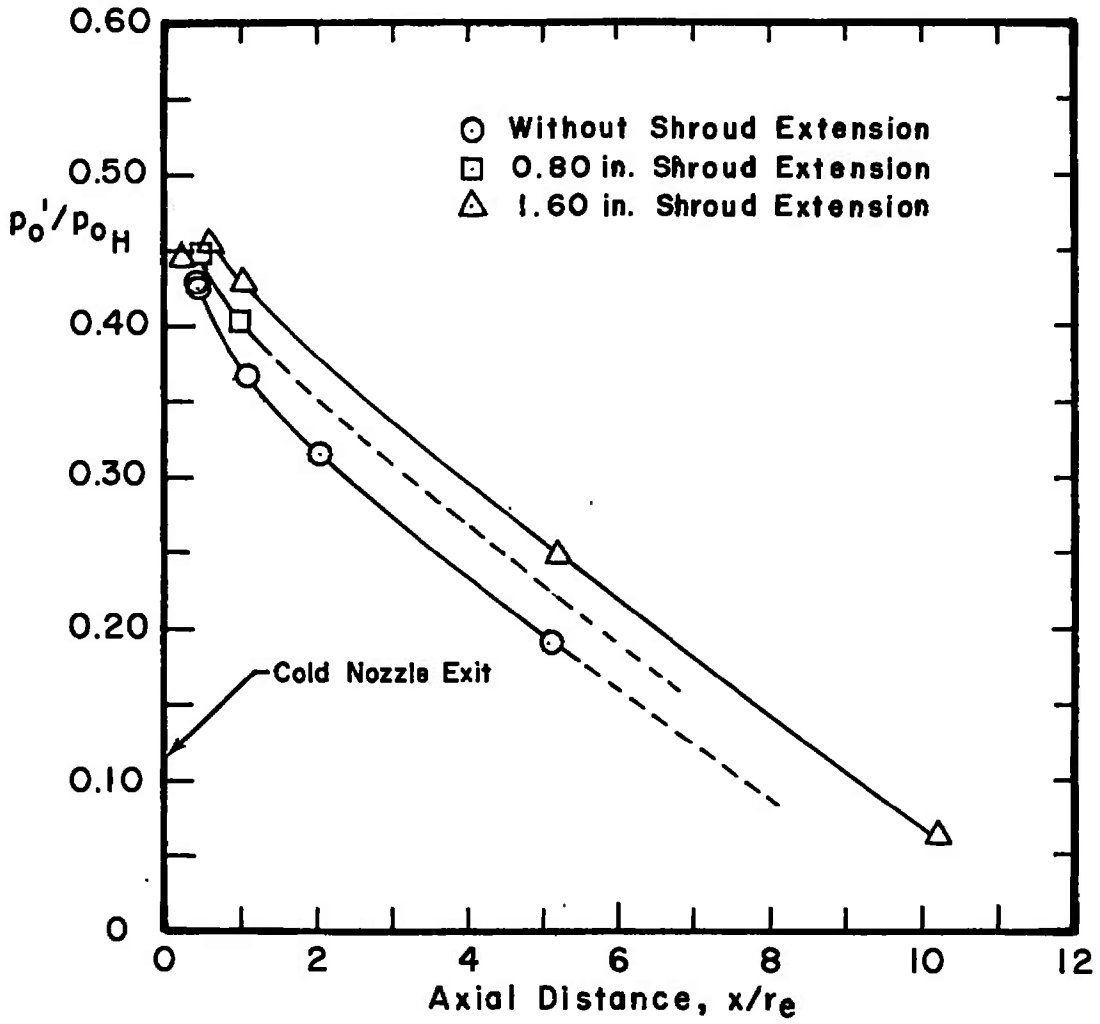

Fig. 16 Effect of Axial Distance on the Model Stagnation Point Pressure with Various Shroud Extensions

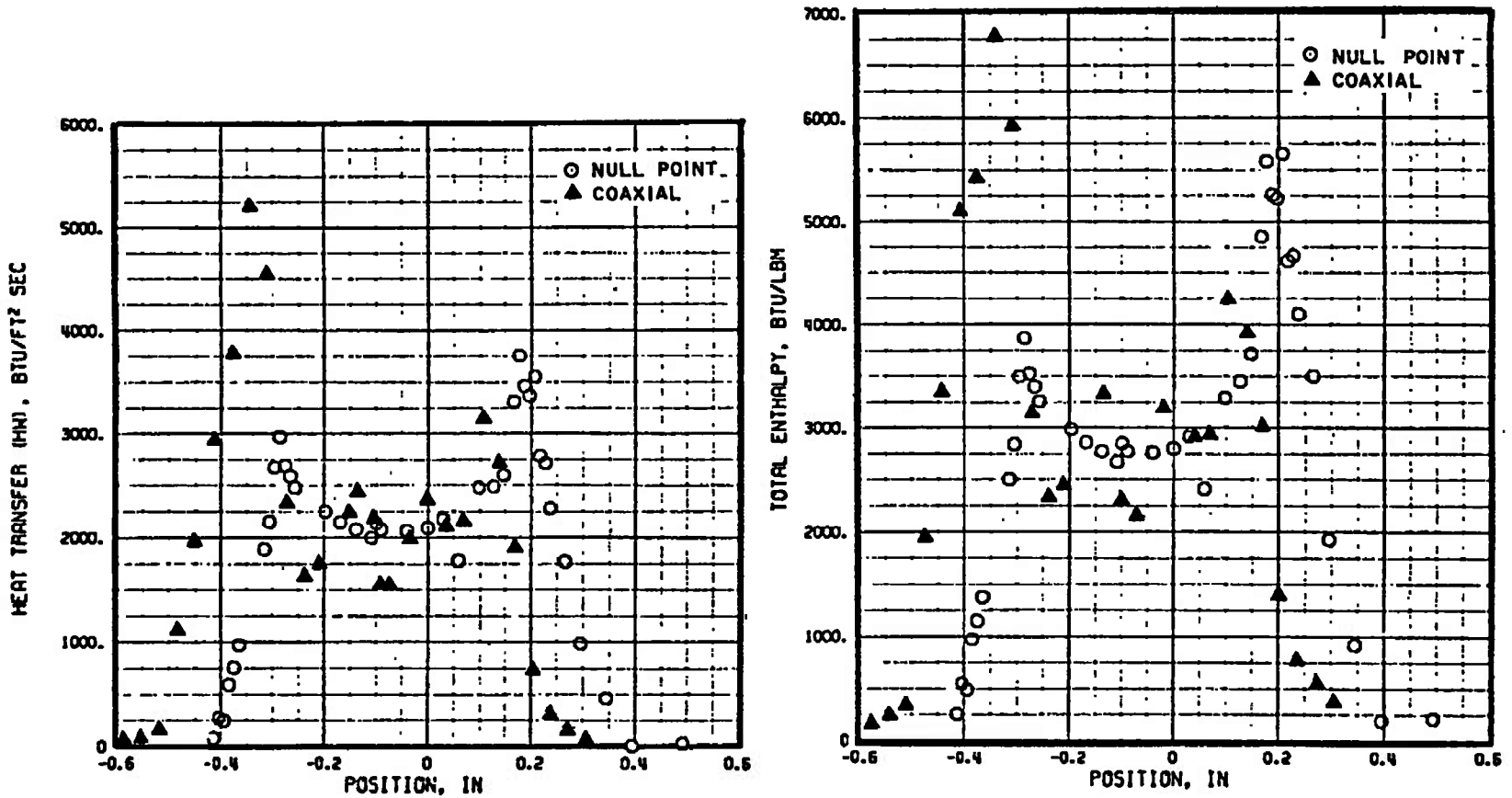

Fig. 17 Stagnation Point Heat Transfer and Enthalpy Distributions, p_{o_H} = 20.1 atm, $H_{o_{HB}}$ = 2350 Btu/lbm

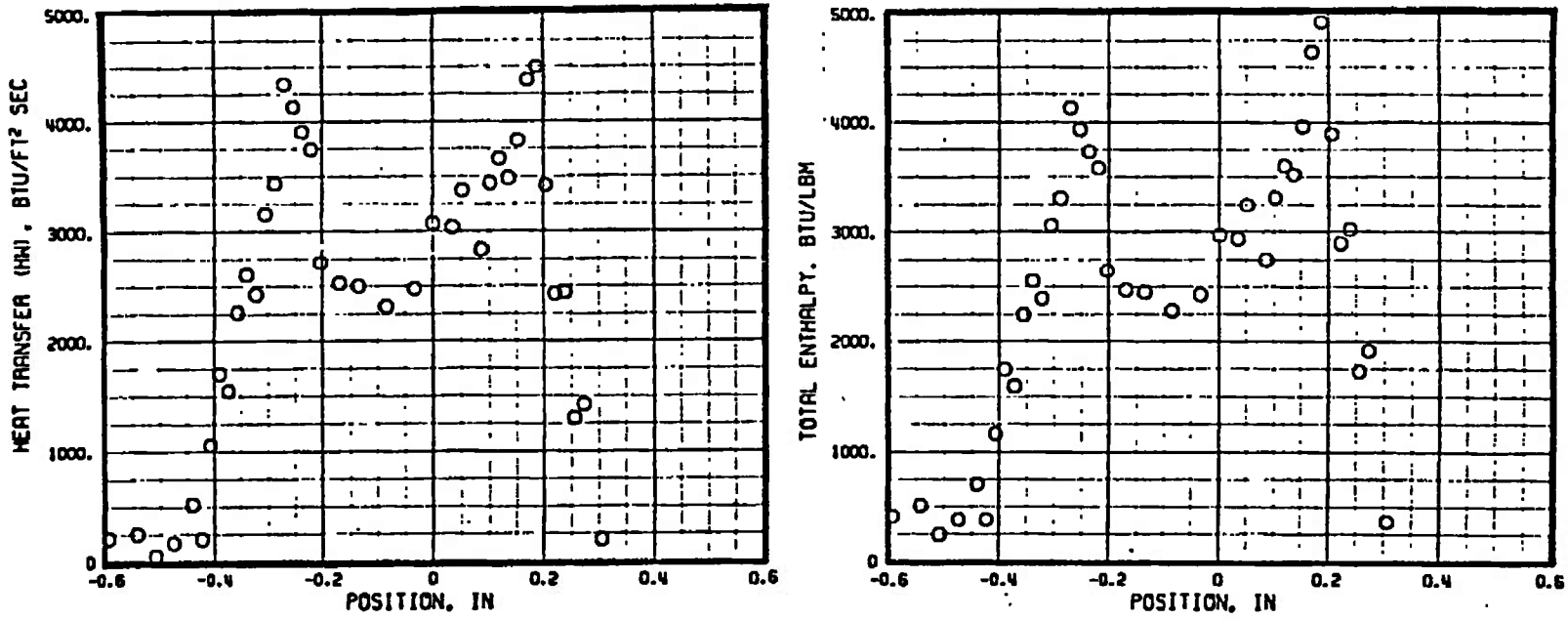

Fig. 18 Stagnation Point Heat Transfer and Enthalpy Distributions, p_{o_H} = 42.9 atm, $H_{o_{HB}}$ = 2091 Btu/lbm

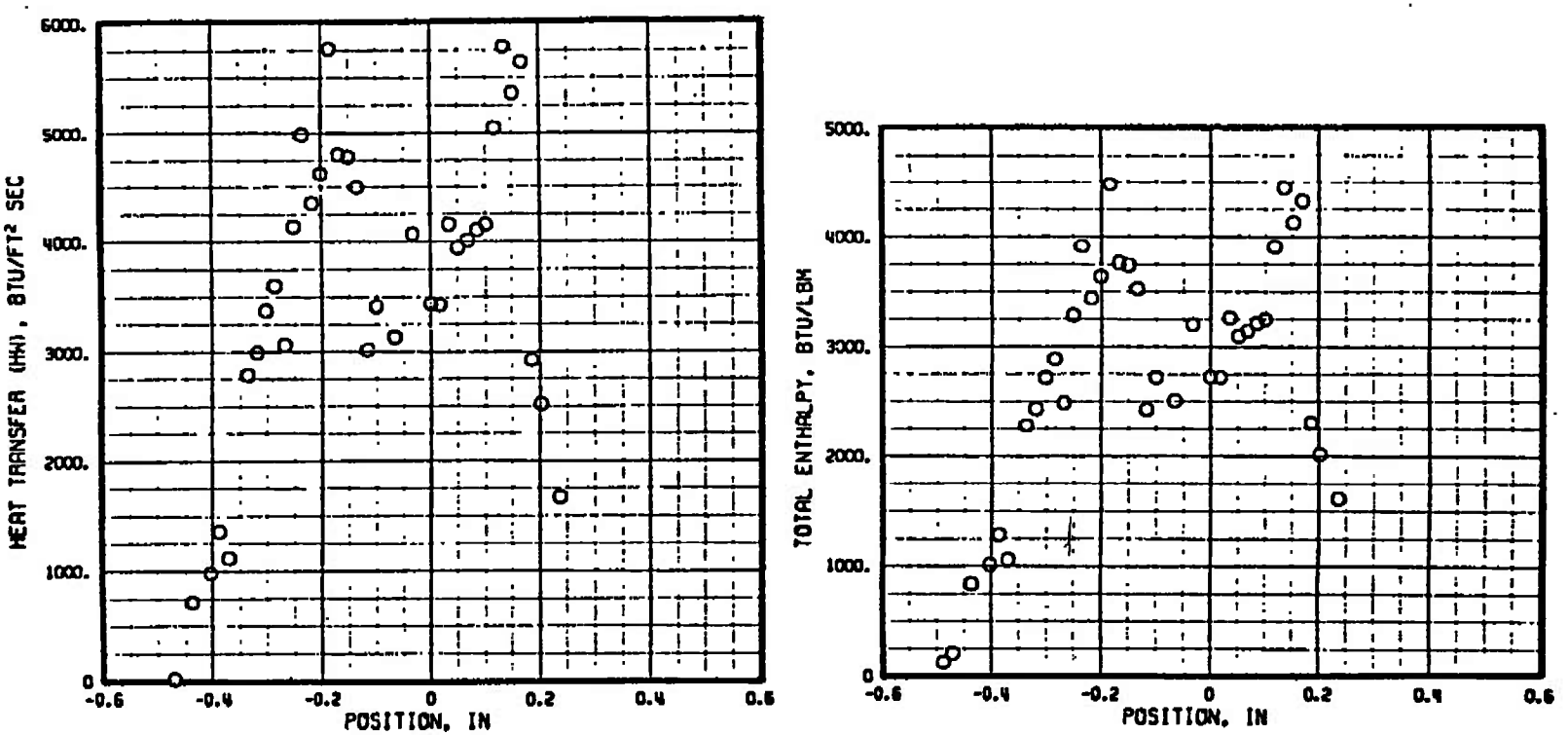

Fig. 19 Stagnation Point Heat Transfer and Enthalpy Distributions, p_{o_H} = 60.4 atm, $H_{o_{HB}}$ = 2110 Btu/lbm

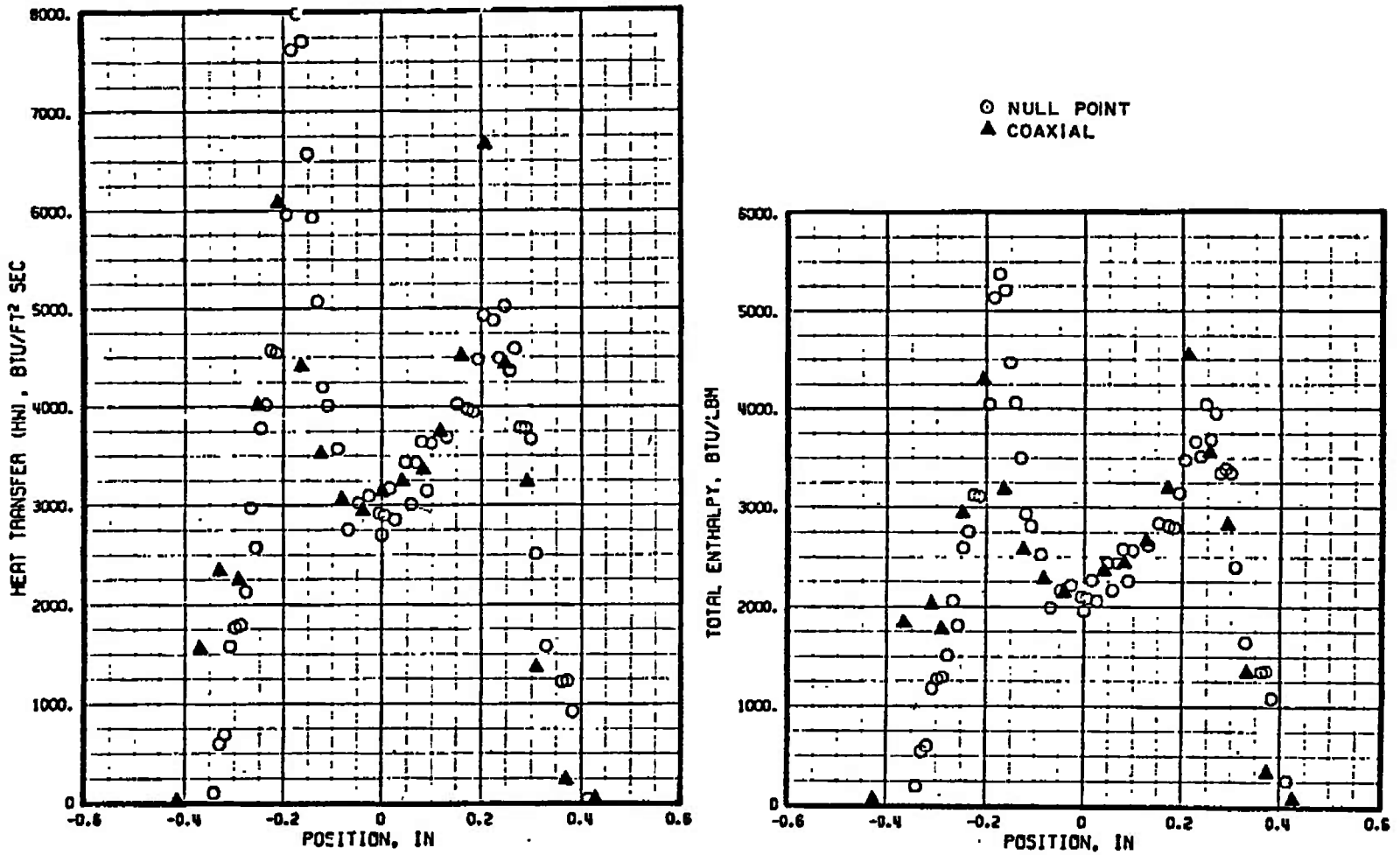

Fig. 20 Stagnation Point Heat Transfer and Enthalpy Distributions, p_{o_H} = 80.1 atm, $H_{o_{HB}}$ = 1890 Btu/lbm

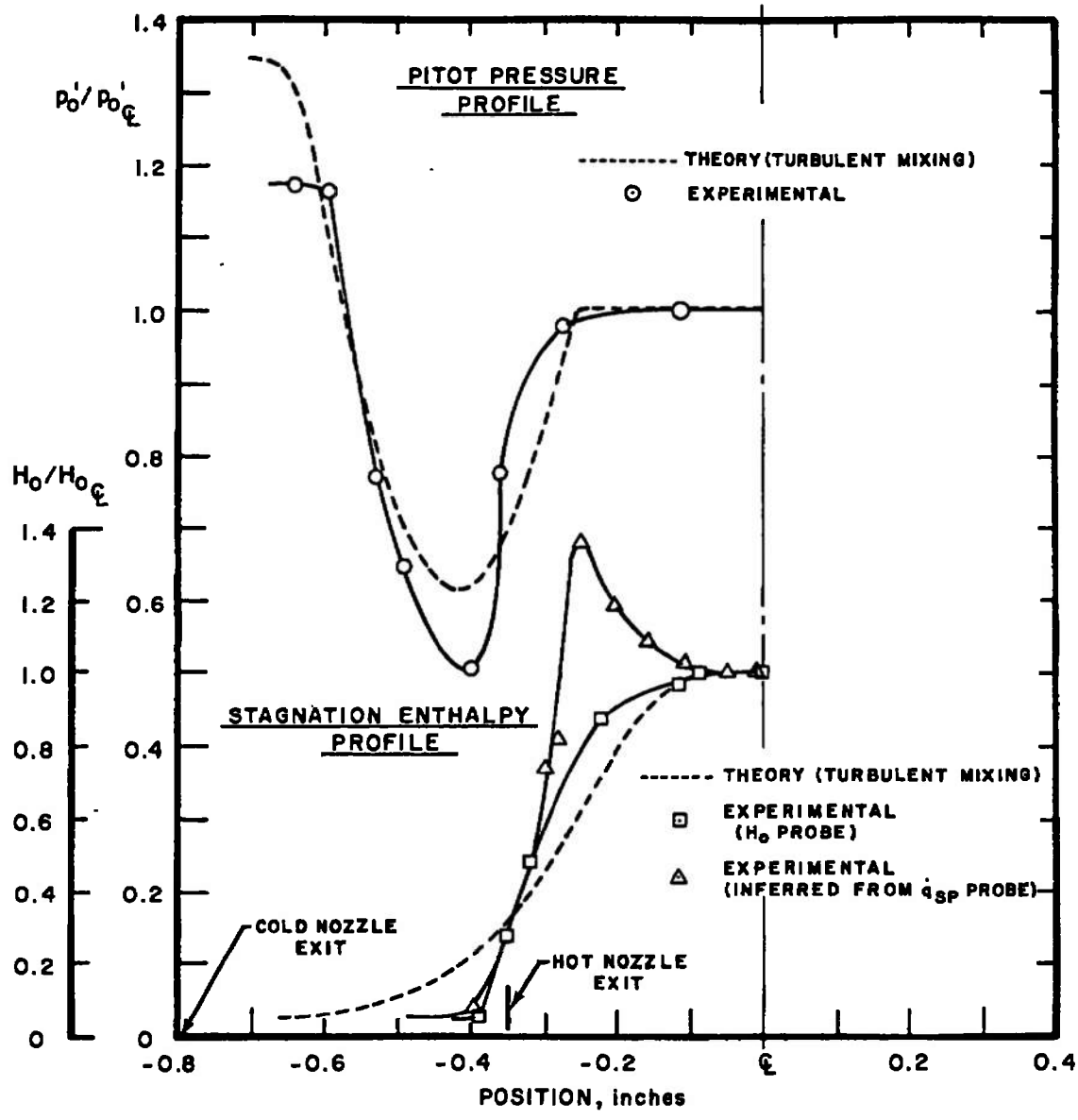

Fig. 21 Comparison of Theoretical and Experimental Profiles of Pitot Pressure and Stagnation Enthalpy, p_{o_H} = 20.1 atm, $H_{o_{HB}}$ = 2350 Btu/lbm

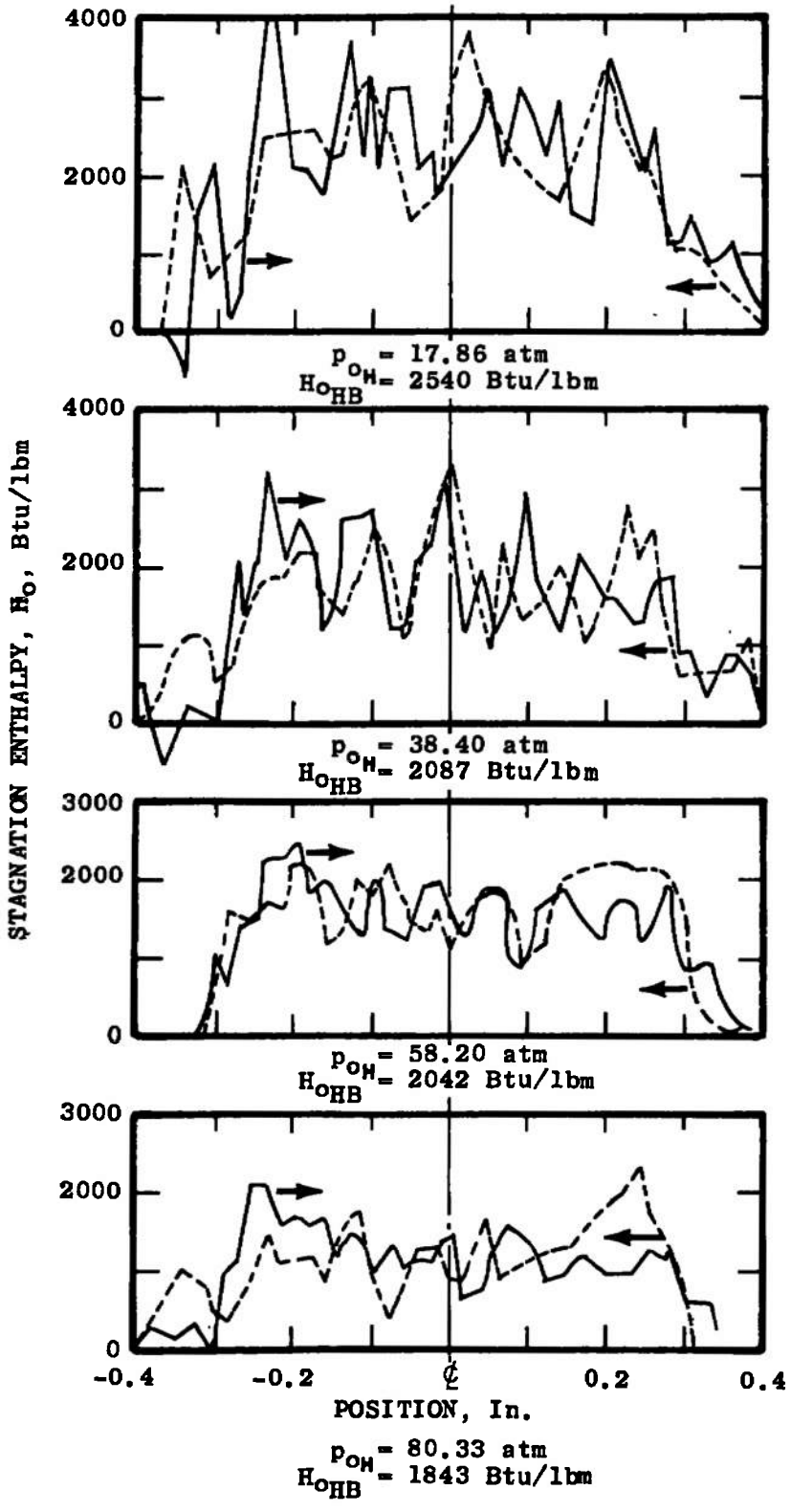

Fig. 22 Unsmoothed-Uncorrected Enthalpy Probe Data

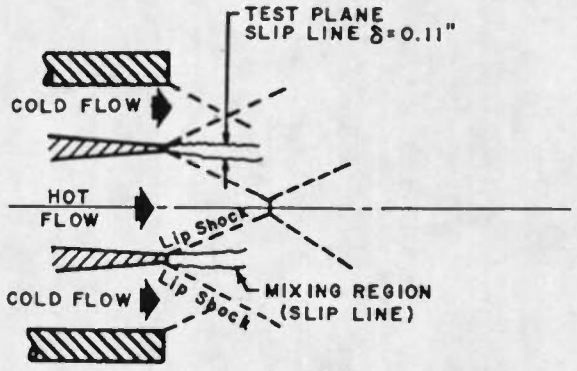

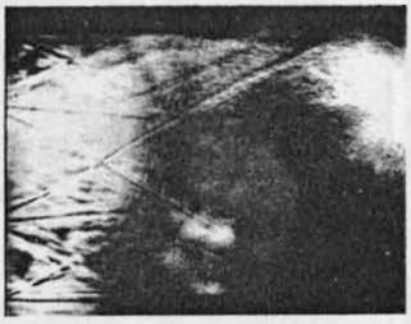

No Shroud Extension

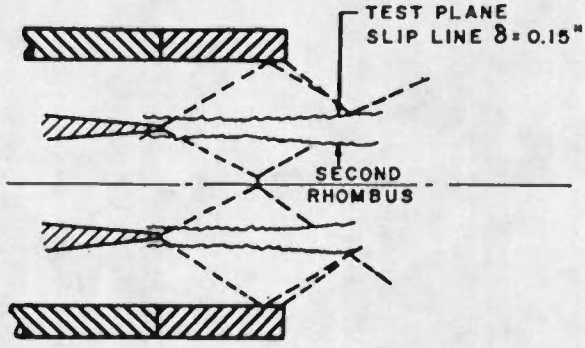

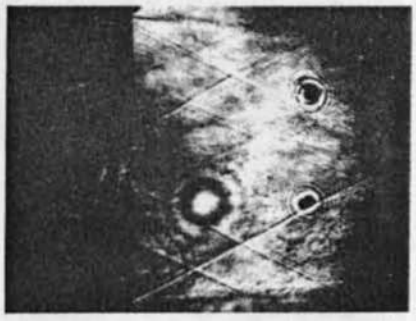

0.80 Inch Shroud Extension

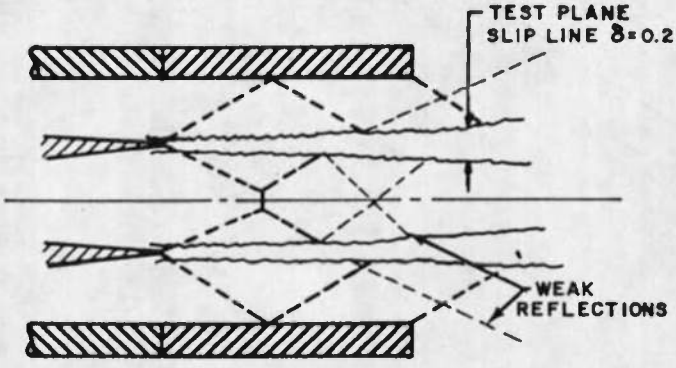

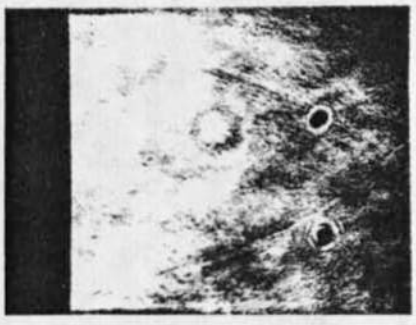

1.60 Inch Shroud Extension

Fig. 23 Shadowgraphs and Sketches of the Flow from Each Shroud Configuration Showing Shock Wave Formations

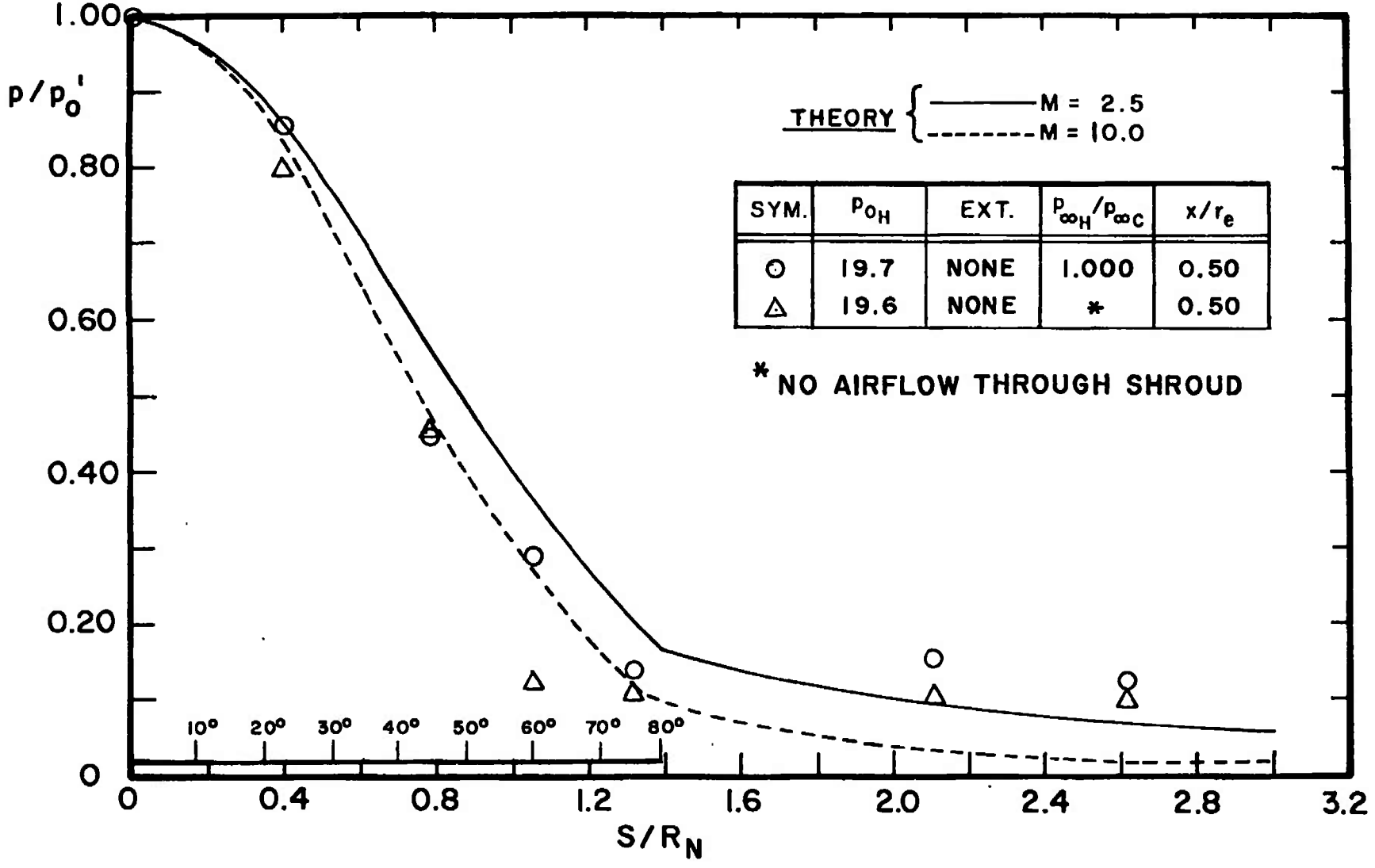

Fig. 24 Pressure Distributions on a 0.50-in. Radius Model with and without a Coaxial Air Jet (Cold Flow)

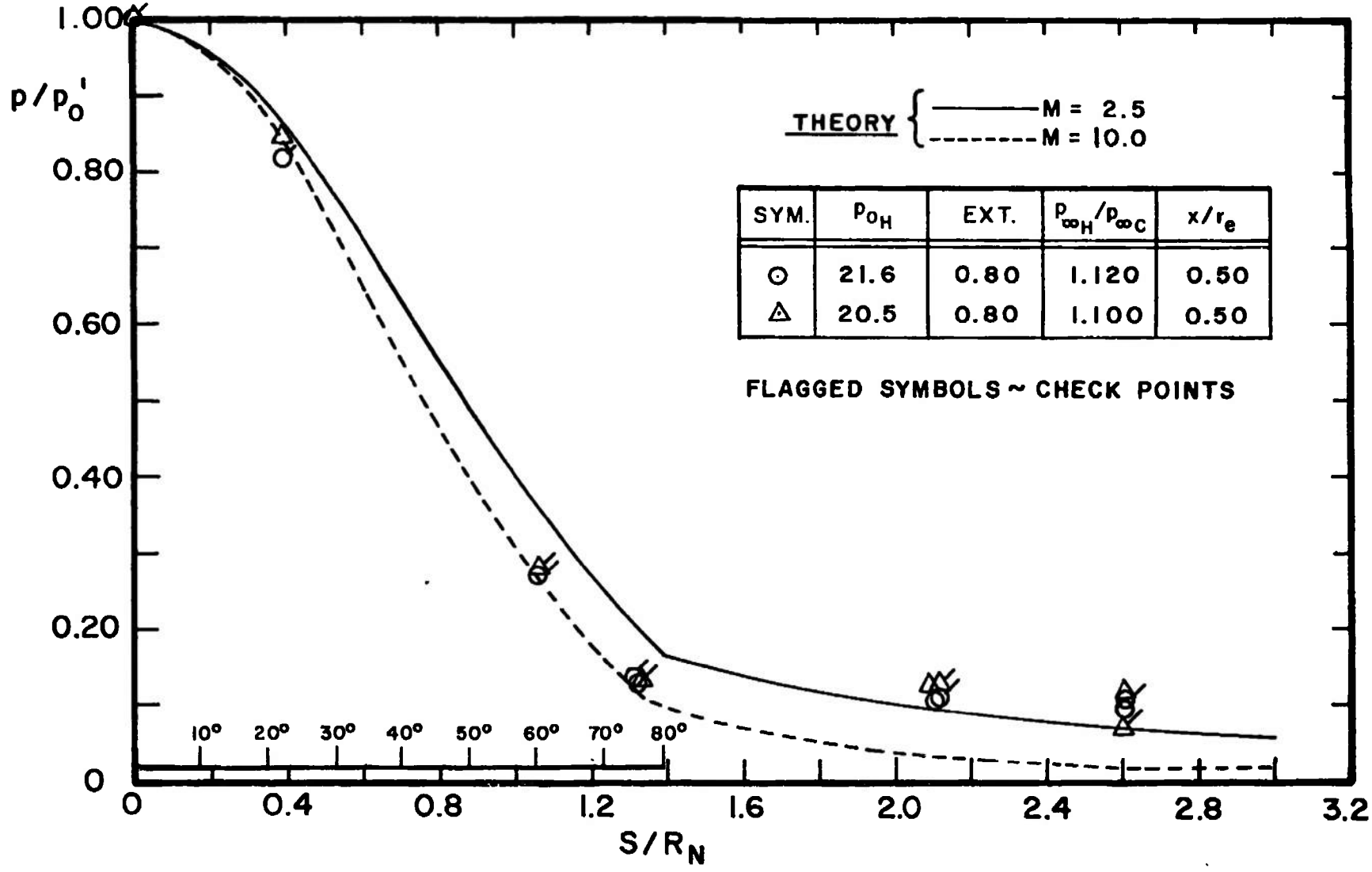

Fig. 25 Pressure Distributions on a 0.50-in. Radius Model Showing Data Repeatability

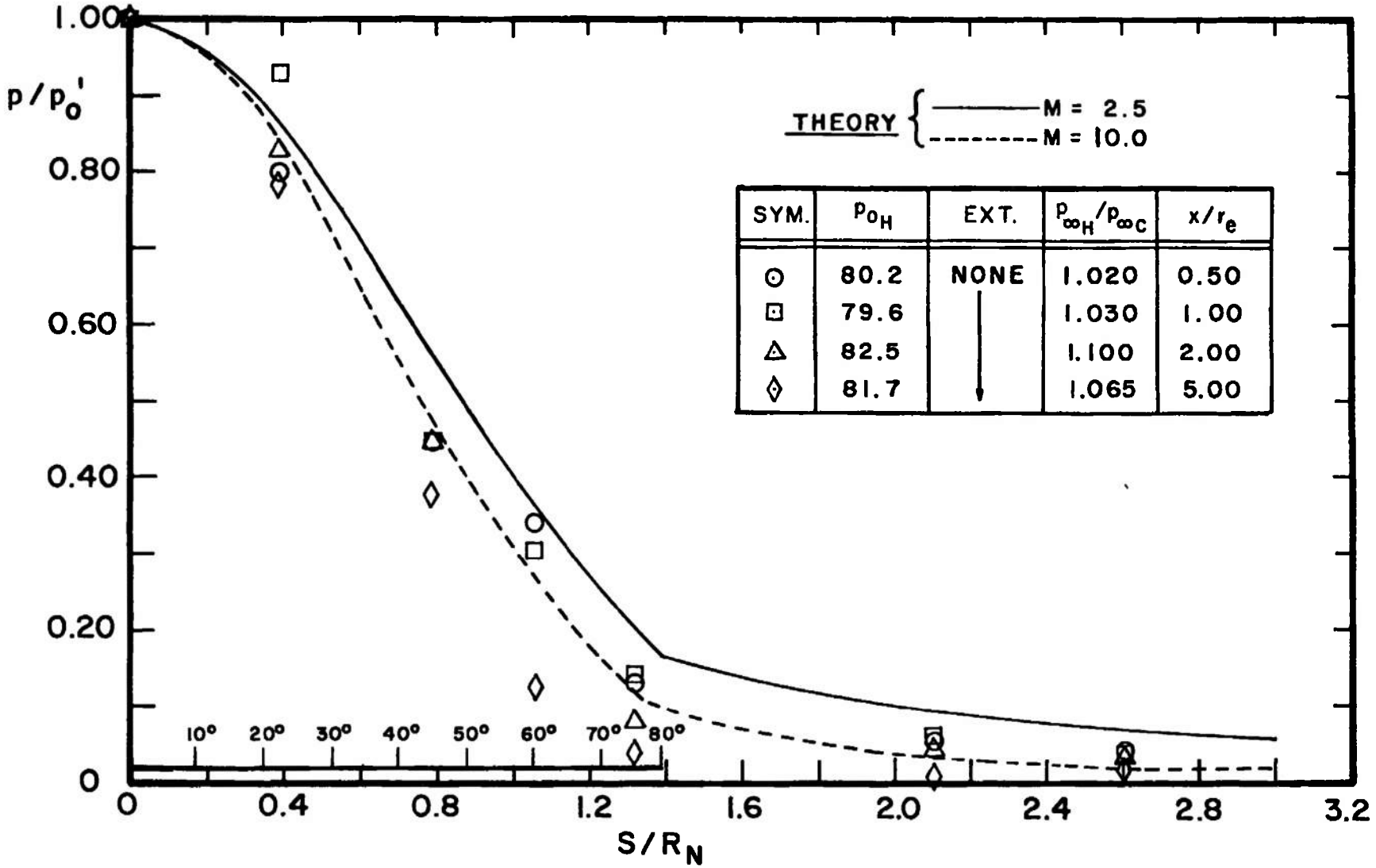

Fig. 26 Pressure Distributions on a 0.50-in. Radius Model at Various x/r_e with No Shroud Extension

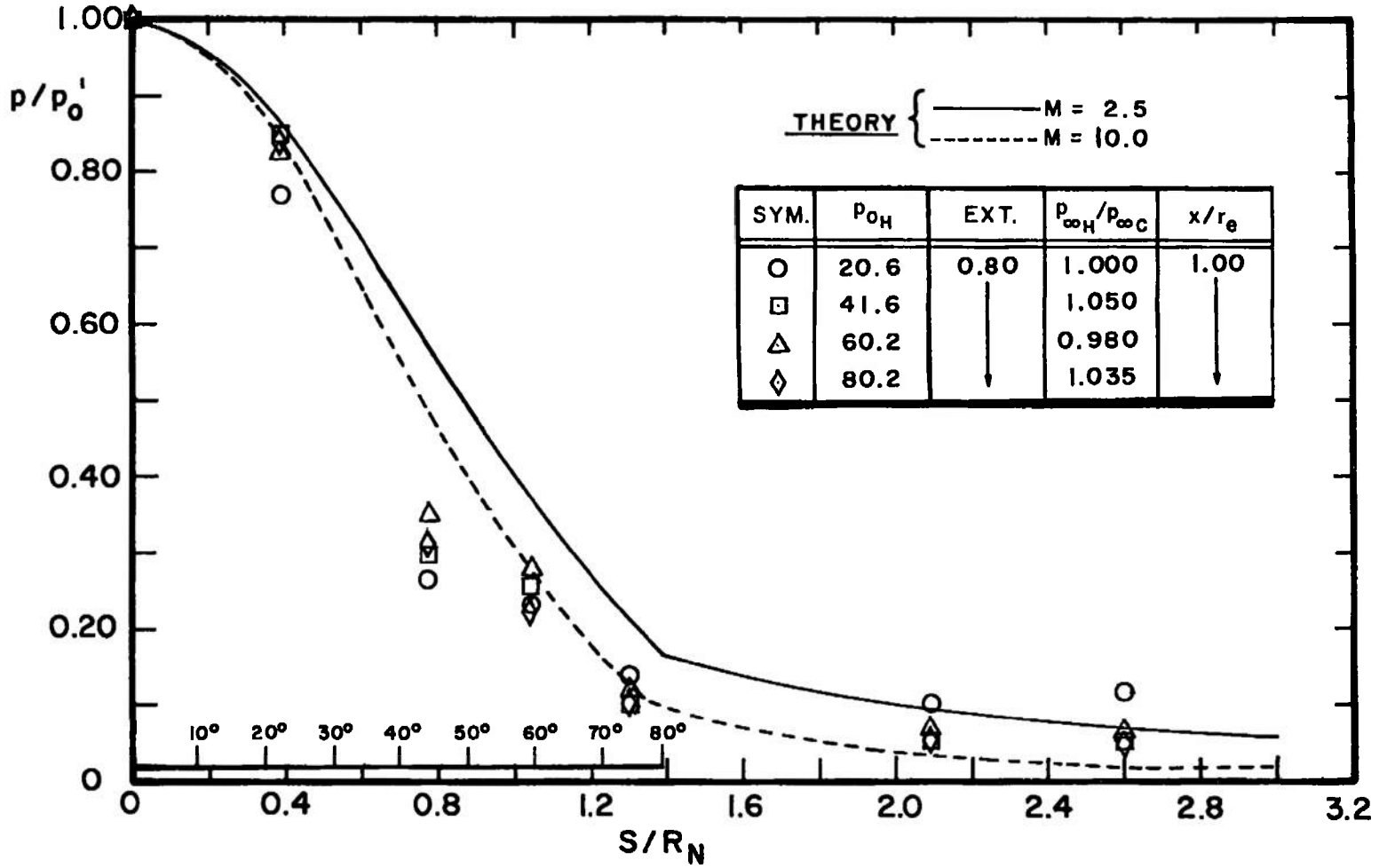

a. Variation with Arc Heater Stagnation Pressure

Fig. 27 Pressure Distributions on a 0.50-in. Radius Model with a 0.80-in. Shroud Extension

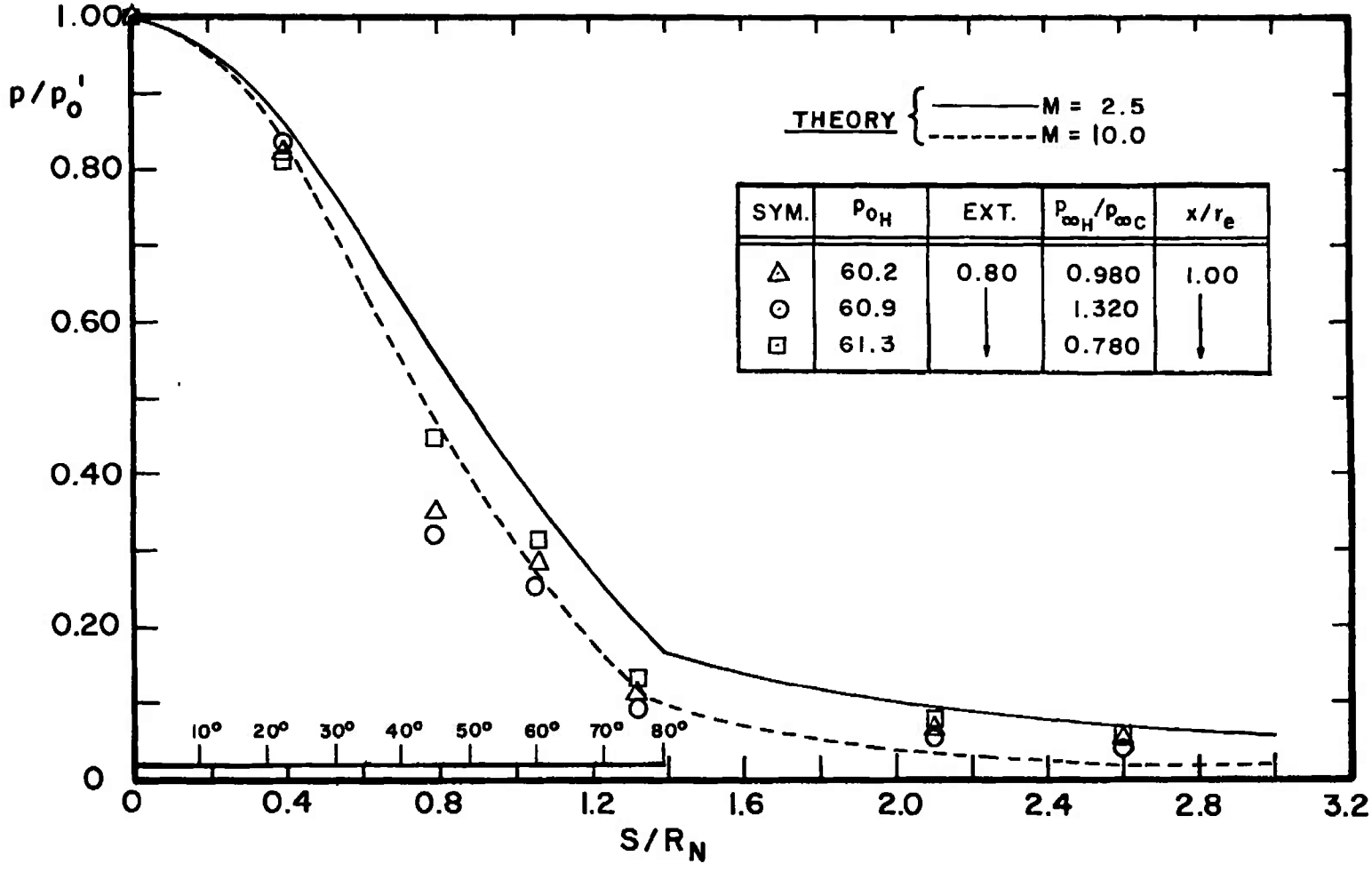

b. Variation with Shroud Pressure
Fig. 27 Concluded

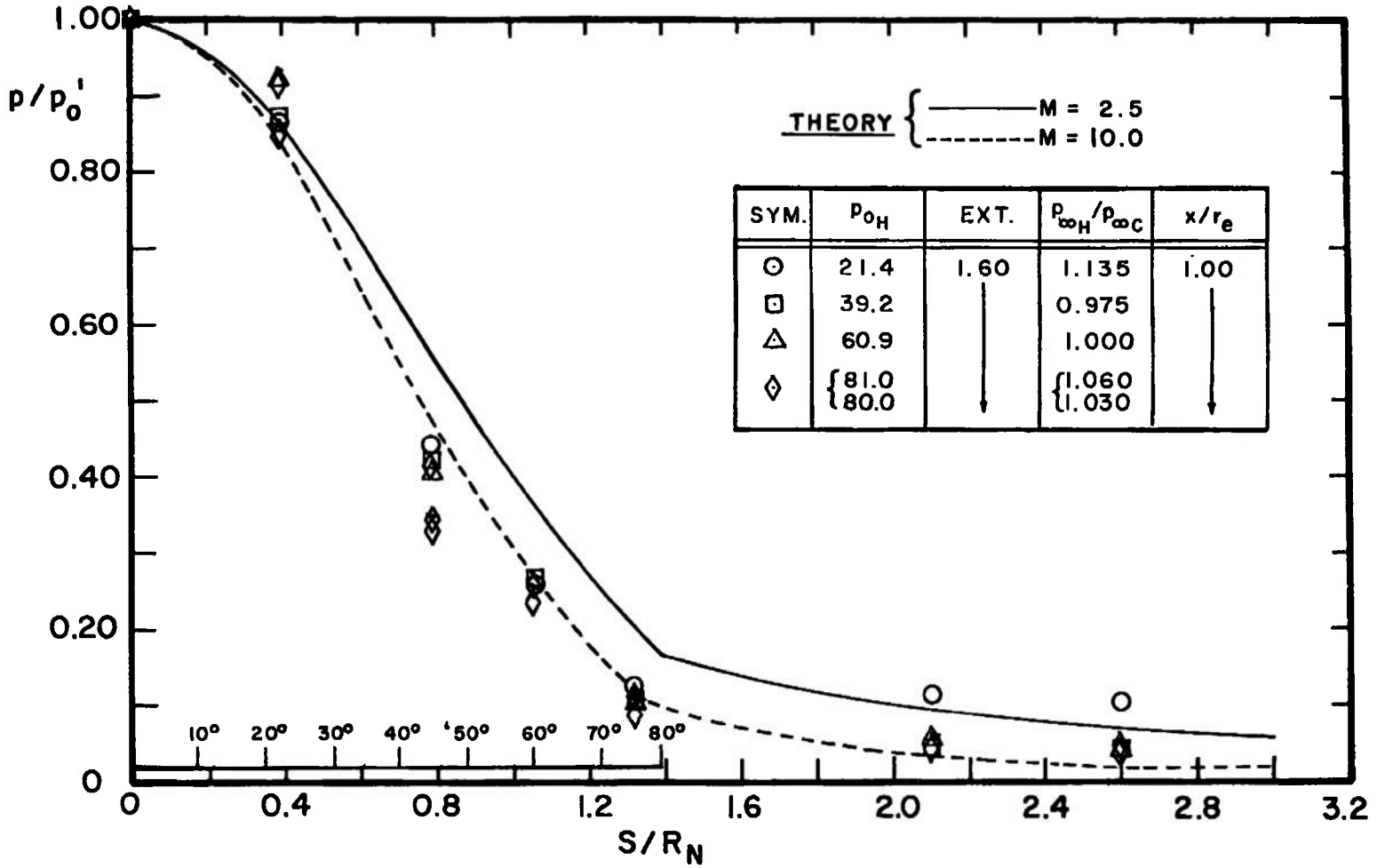

a. Variation with Arc Heater Stagnation Pressure

Fig. 28 Pressure Distributions on a 0.50-in. Radius Model with a 1.60-in. Shroud Extension

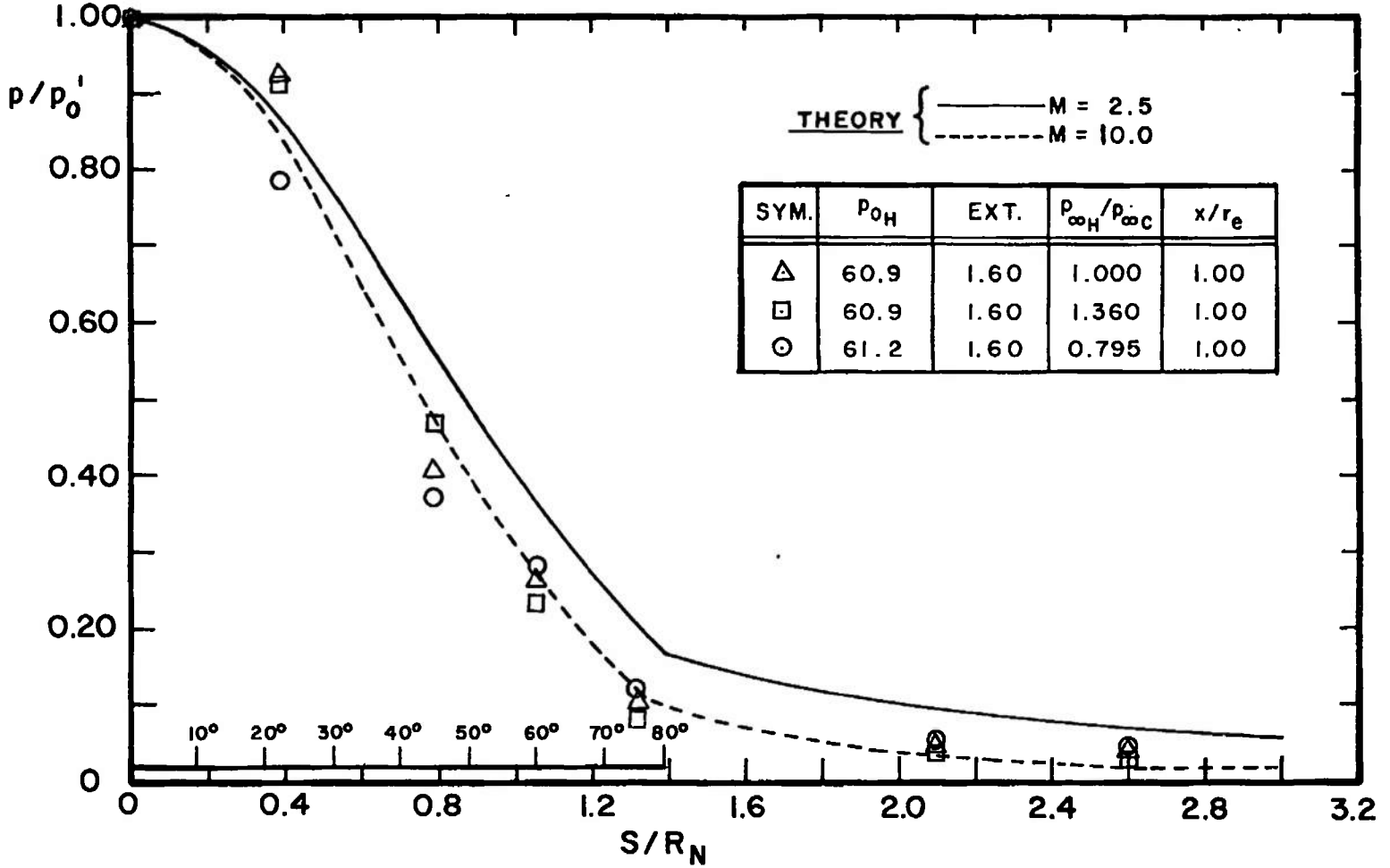

b. Variation with Shroud Pressure
Fig. 28 Concluded

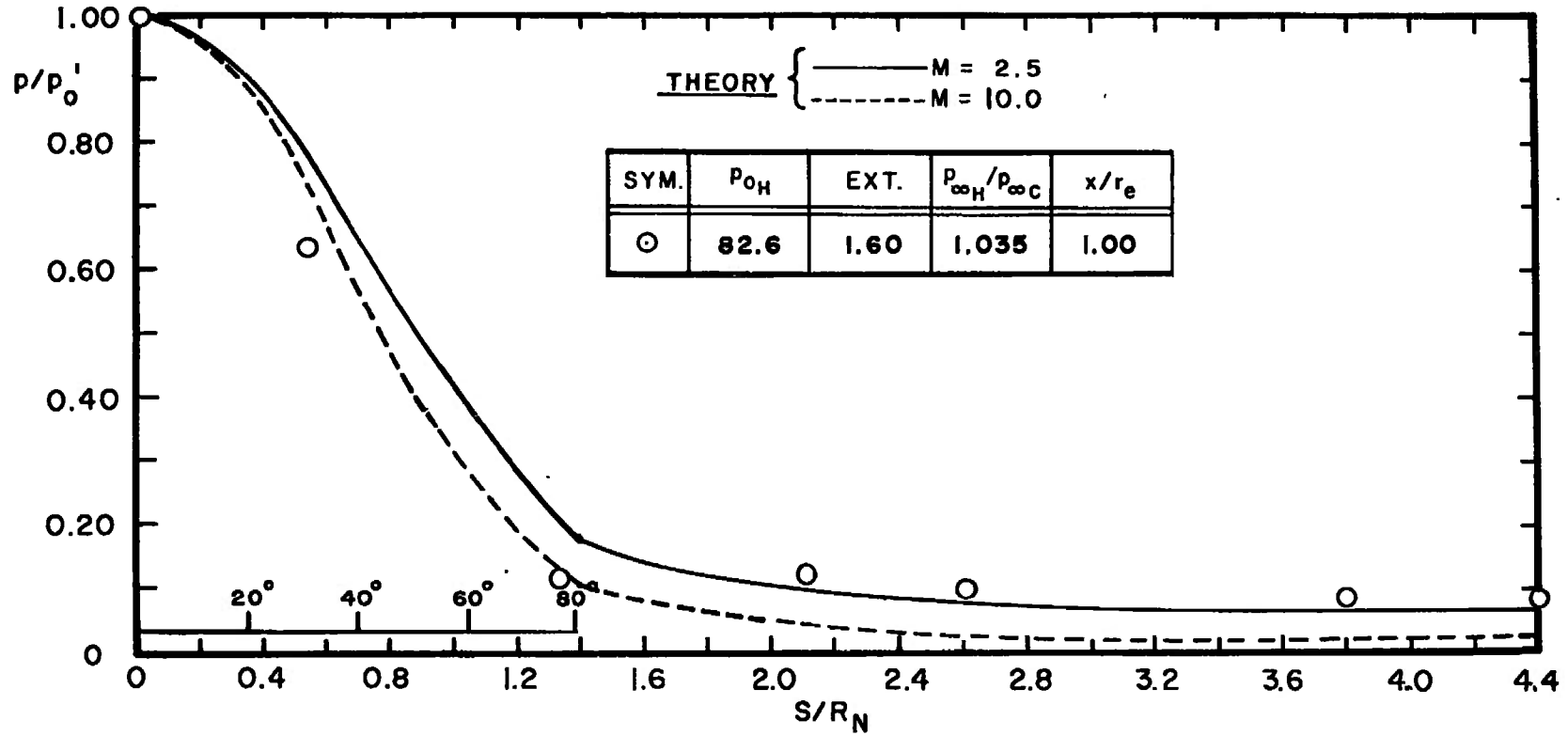

Fig. 29 Pressure Distributions on a 0.25-in. Radius Model with a 1.6-in. Shroud Extension Operating at High Stagnation Pressure

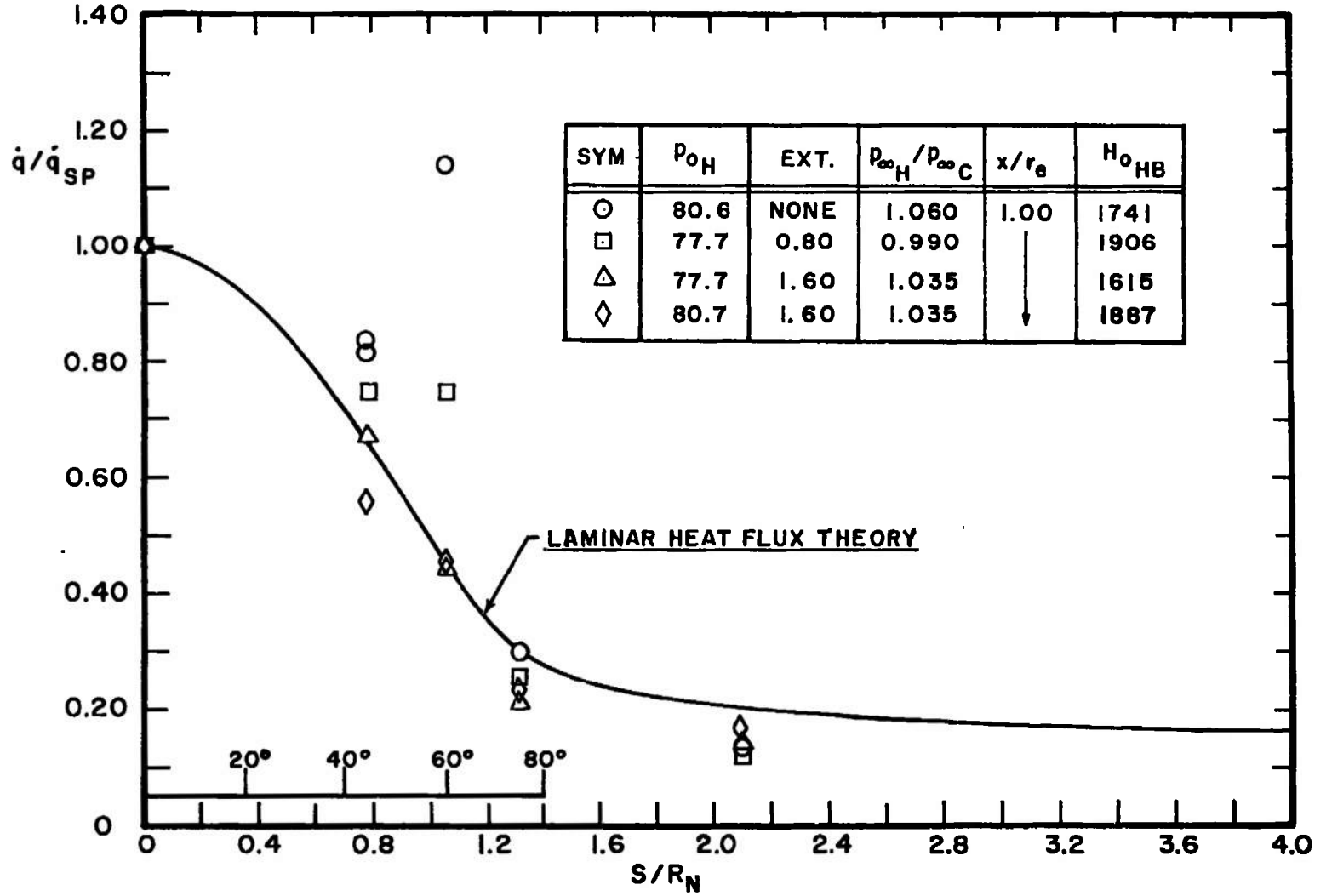

Fig. 30 Heat Transfer Distributions on a 0.50-in. Radius Model at High Stagnation Pressure

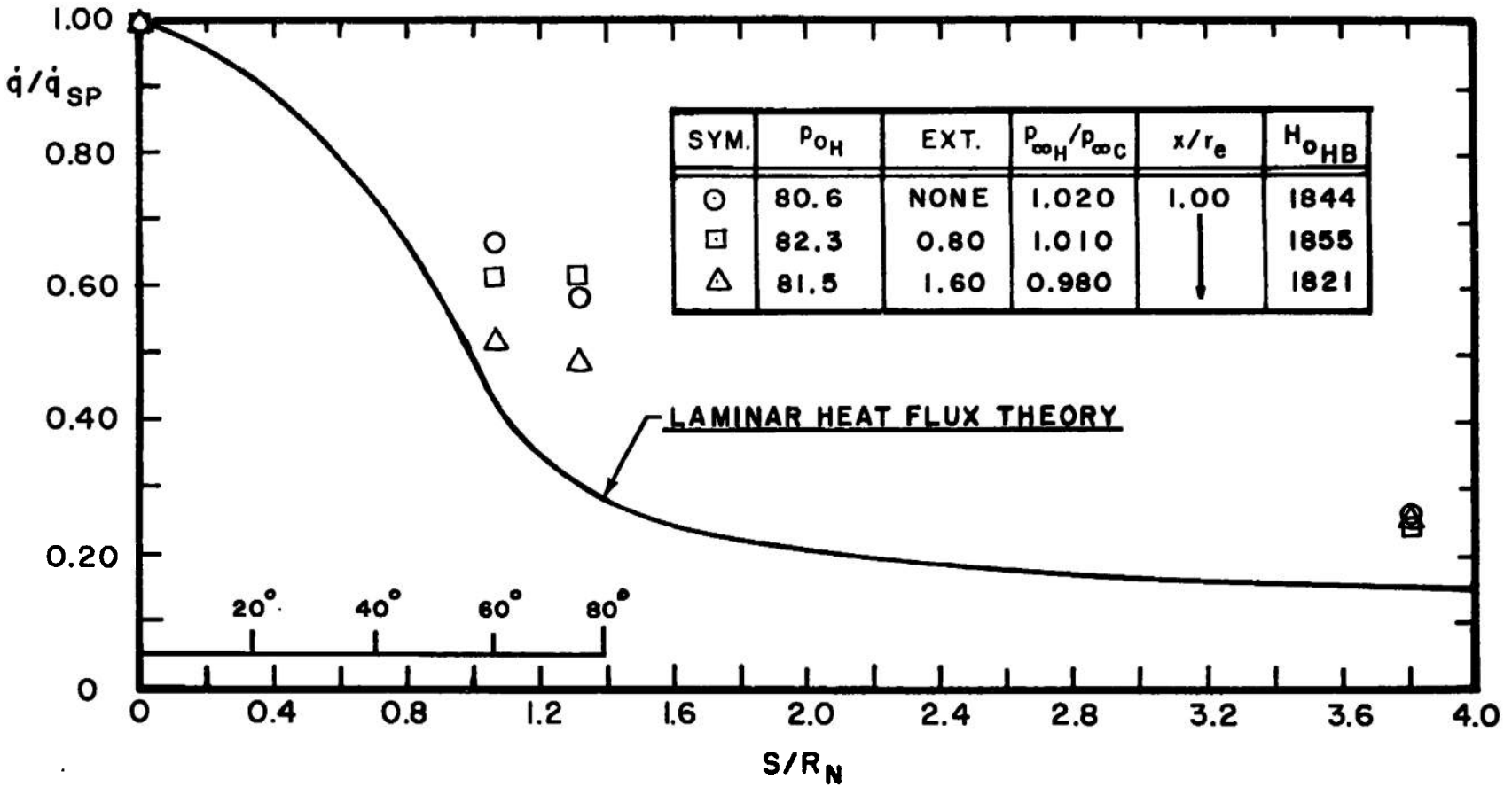

Fig. 31 Heat Transfer Distributions on a 0.25-in. Radius Model at High Stagnation Pressure

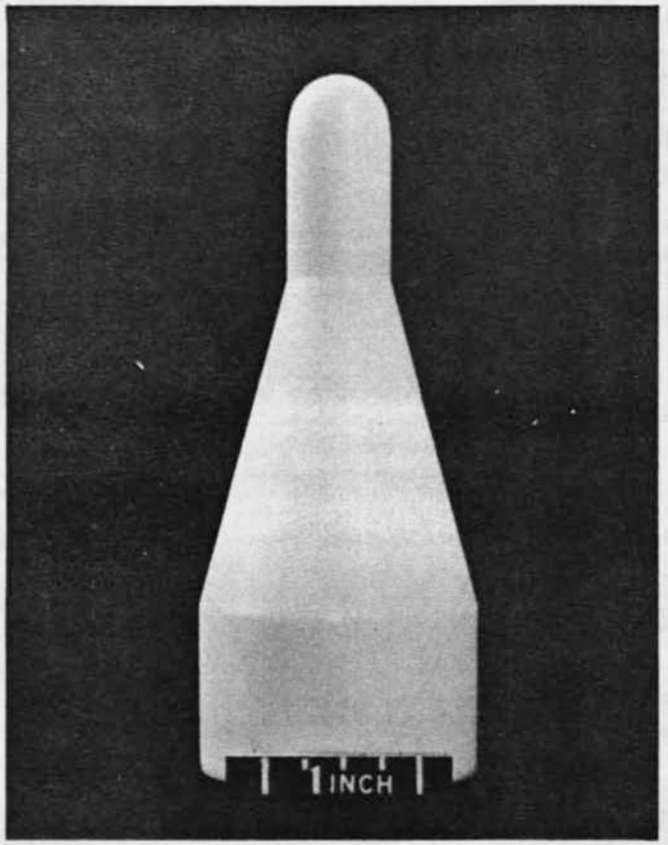

Before Ablation

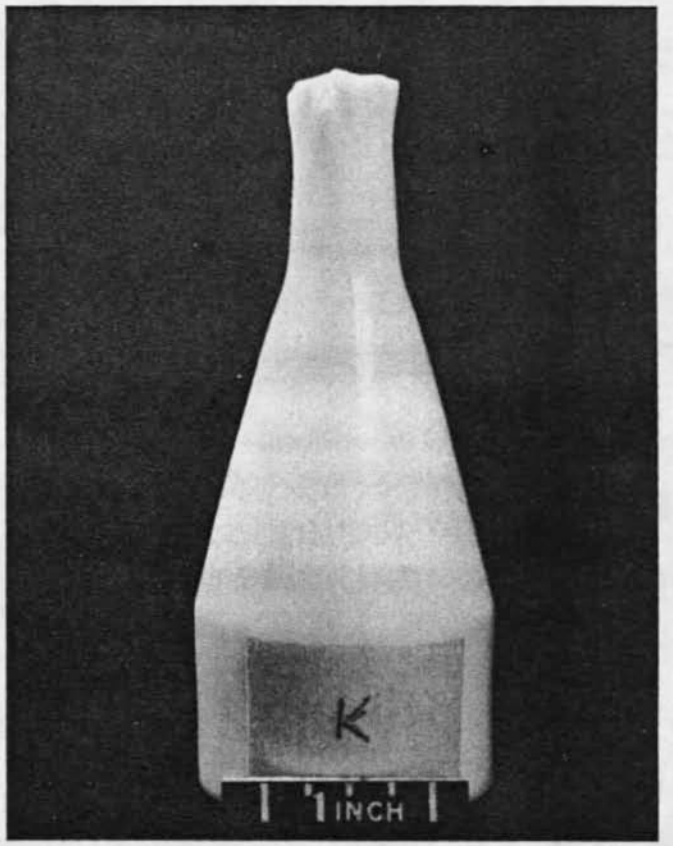

After Ablation

$p_{o}' = 21.2$ atm

$H_{oHB} = 1838$ Btu/lbm

Fig. 32 Photographs of the 0.375-in. Radius Teflon Model before and after Ablation at $p_{oH} = 51$ atm

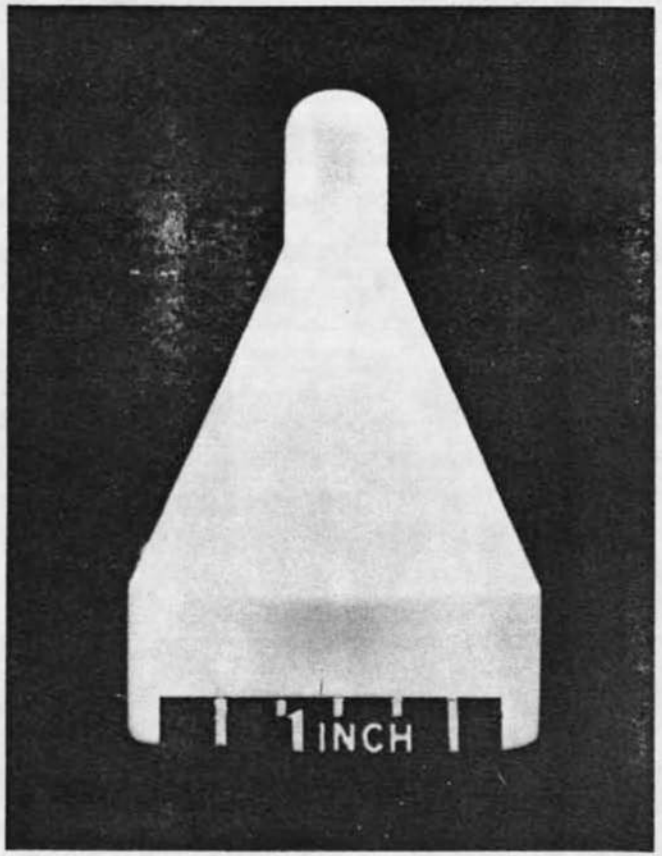

Before Ablation

After Ablation

$p_{o}' = 32.5$ atm

$H_{o_{HB}} = 1796$ Btu/lbm

Fig. 33 Photographs of the 0.250-in. Radius Teflon Model before and after Ablation at $p_{o_H} = 78.9$ atm

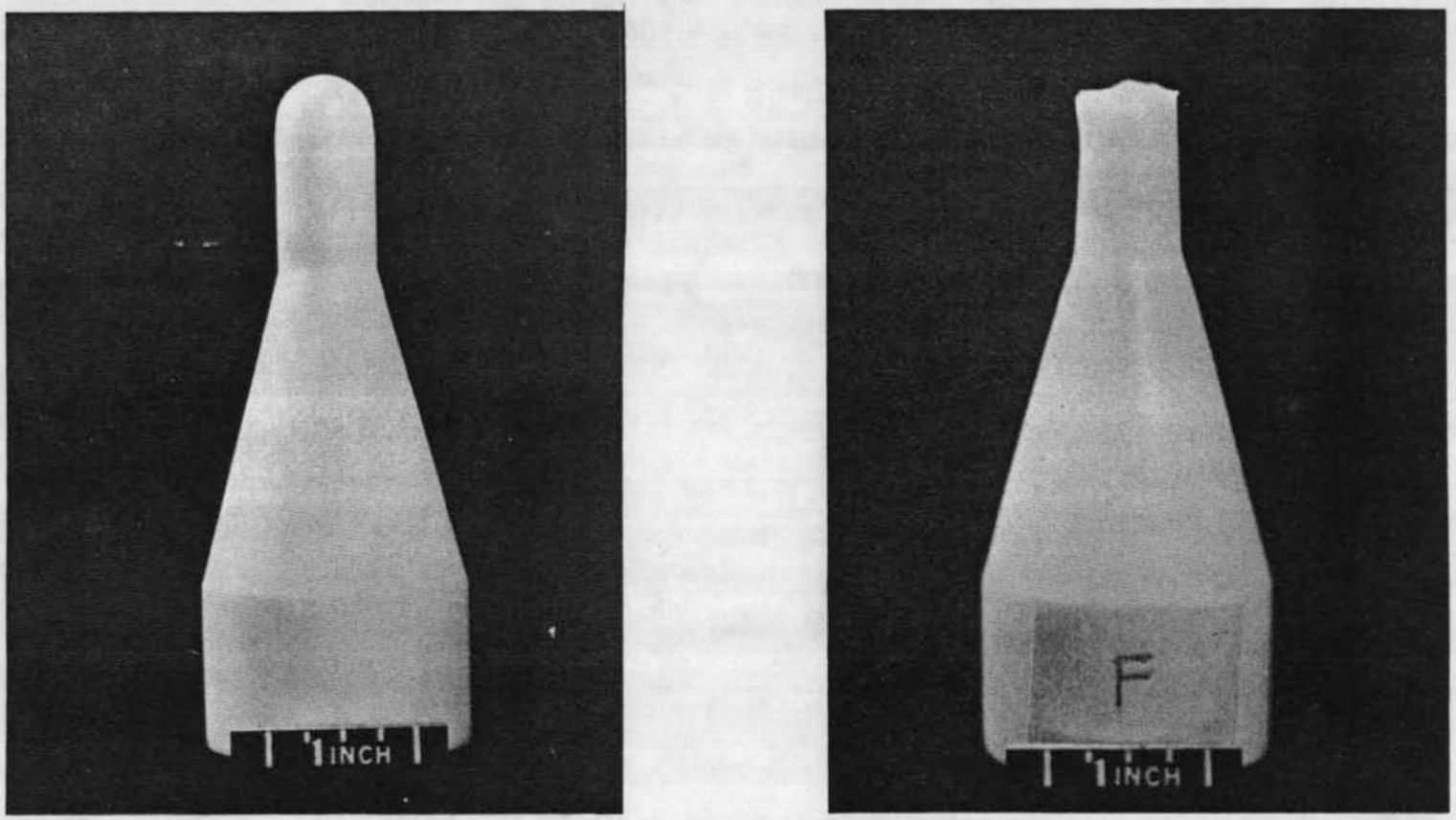

Before Ablation

After Ablation

$p_o' = 33.8$ atm

$H_{o_{HB}} = 1628$ Btu/lbm

Fig. 34 Photographs of the 0.375-in. Radius Teflon Model before and after Ablation at $p_{o_H} = 81.5$ atm

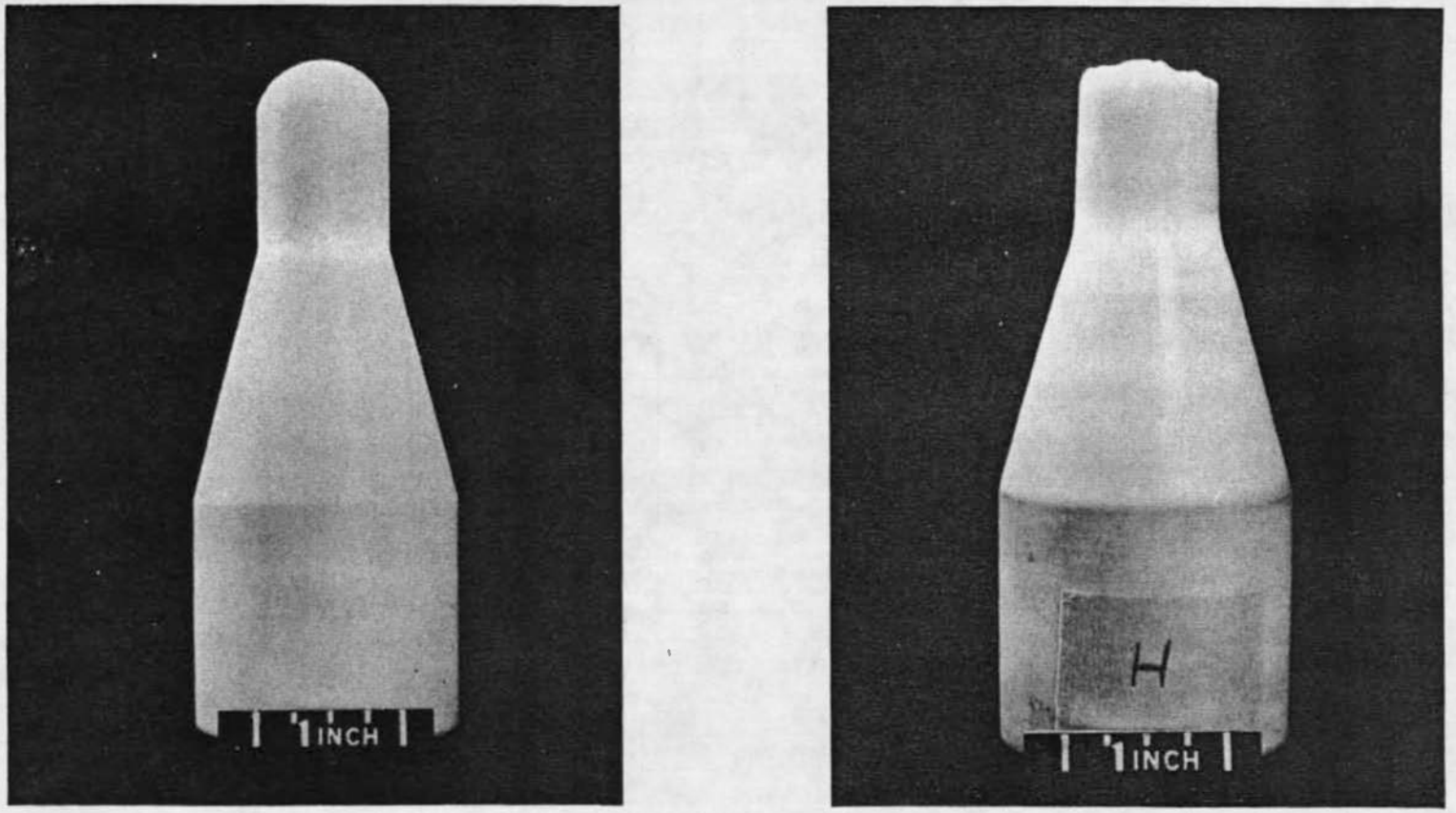

Before Ablation

After Ablation

$p_{o}' = 33.2$ atm

$H_{o_{HB}} = 1651$ Btu/lbm

Fig. 35 Photographs of the 0.500-in. Radius Teflon Model before and after Ablation at $p_{o_H} = 79.9$ atm

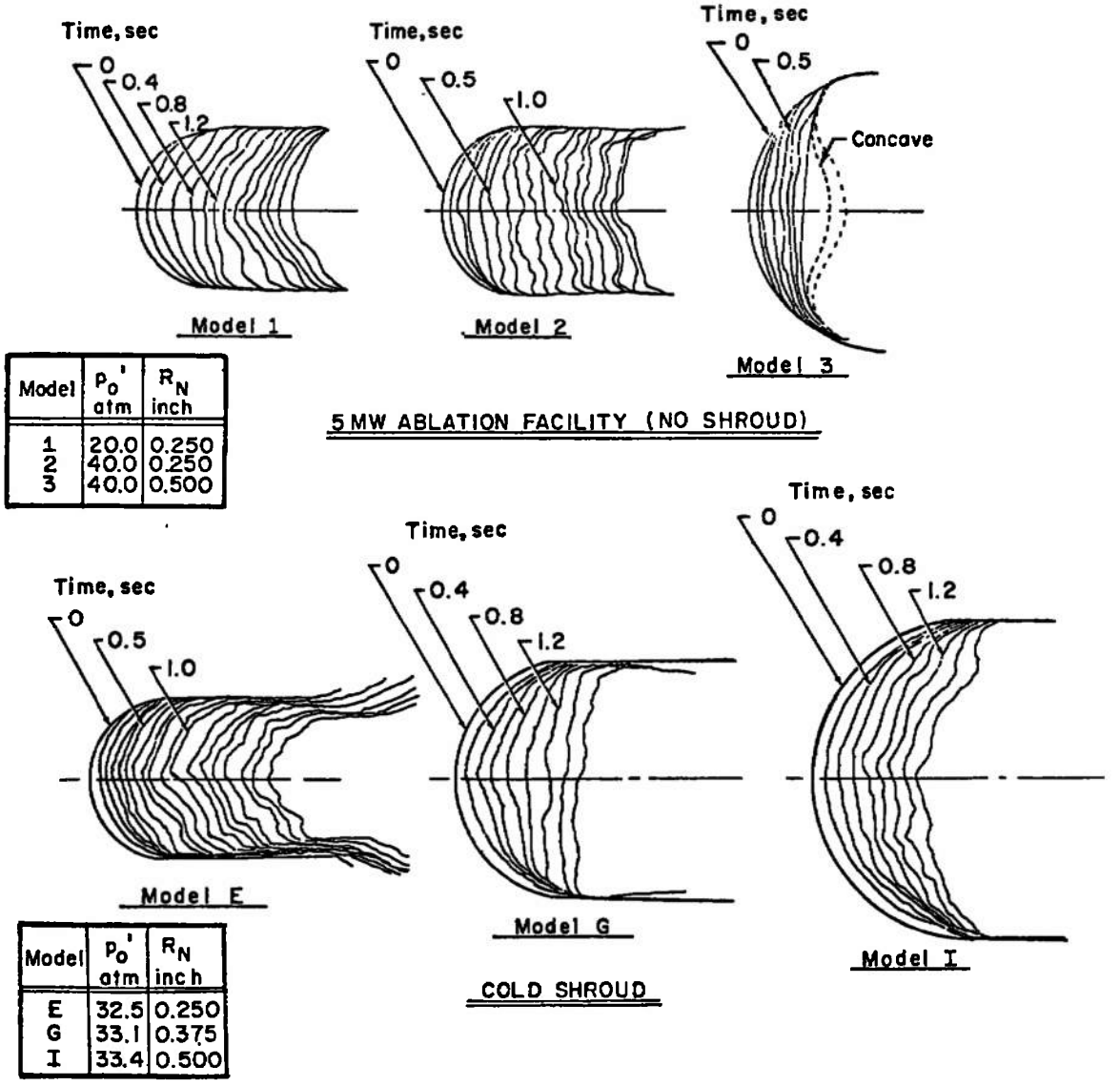

Model	p_o' atm	R_N inch
1	20.0	0.250
2	40.0	0.250
3	40.0	0.500

Model	p_o' atm	R_N inch
E	32.5	0.250
G	33.1	0.375
I	33.4	0.500

Fig. 36 Ablation Profiles of Teflon Models

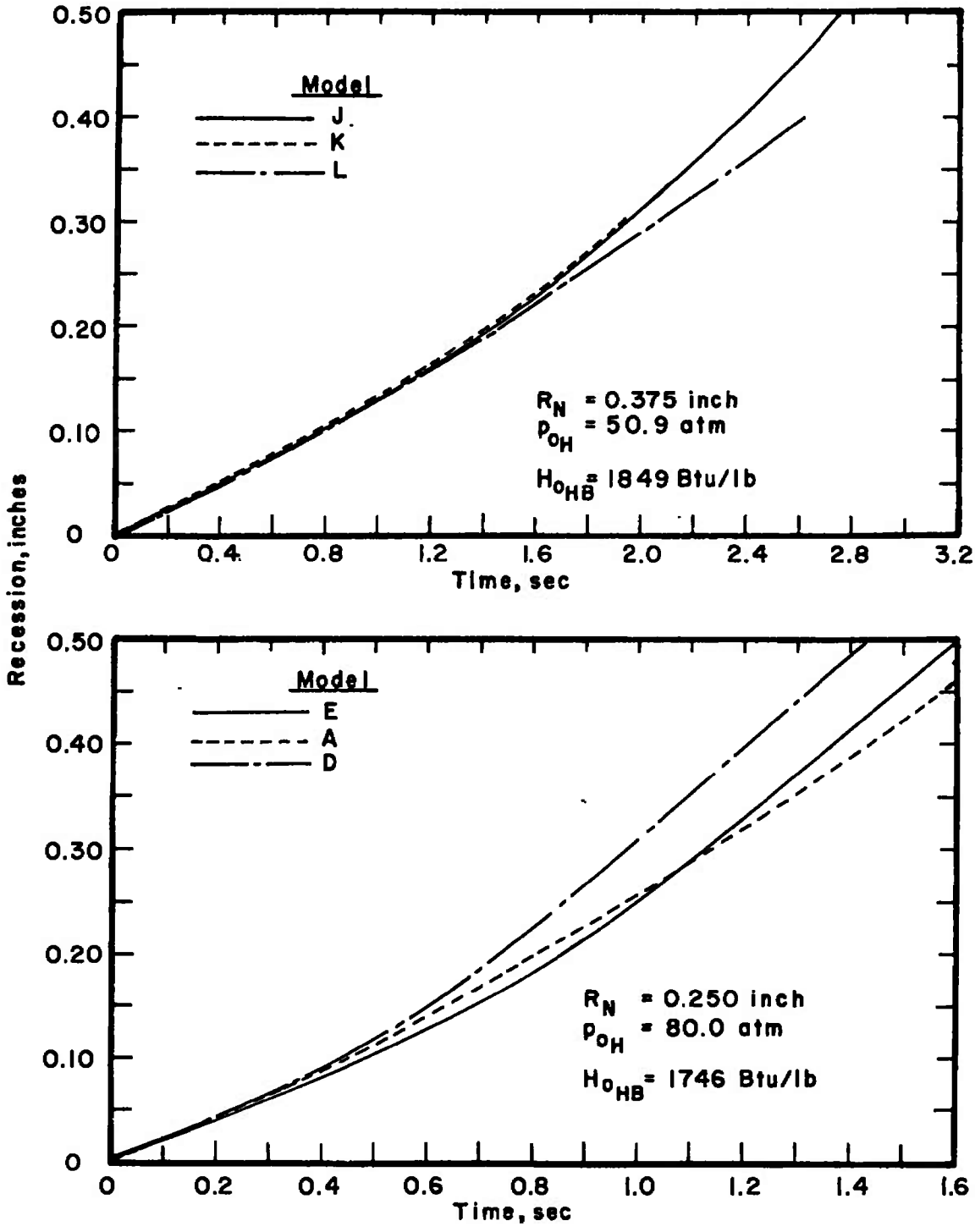

Fig. 37 Ablation of Teflon Models Showing the Recession with Time

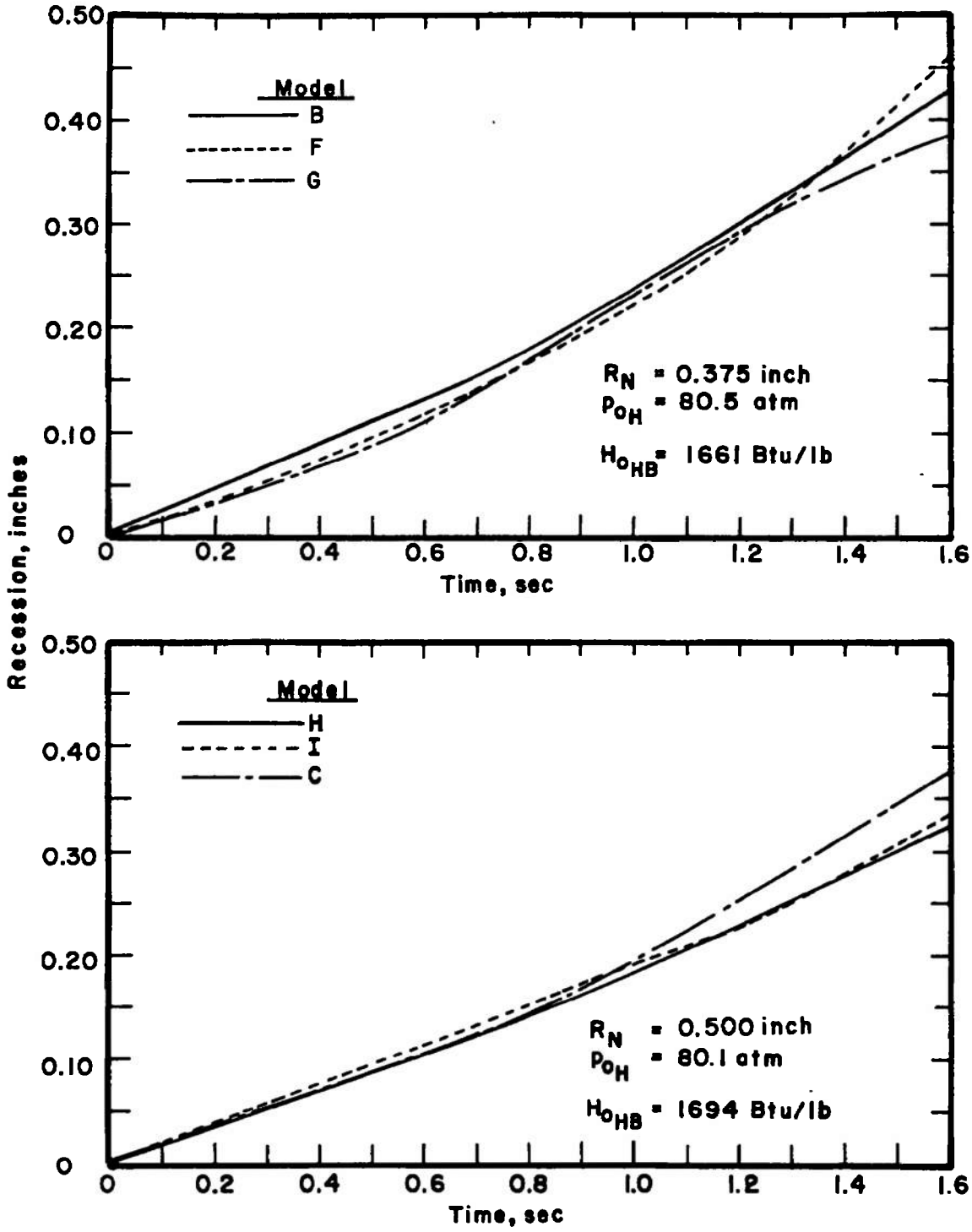

Fig. 37 Concluded

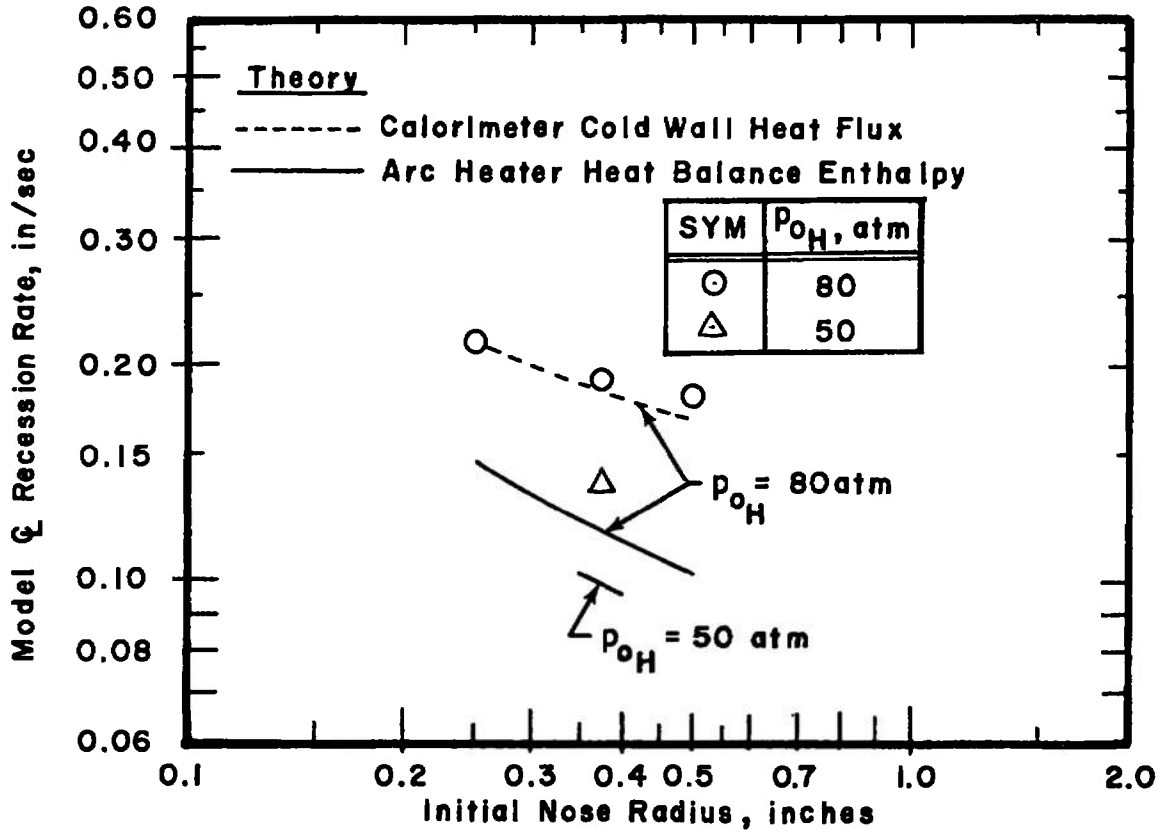

Fig. 38 Ablation Rate of Teflon Compared with a Correlation Parameter

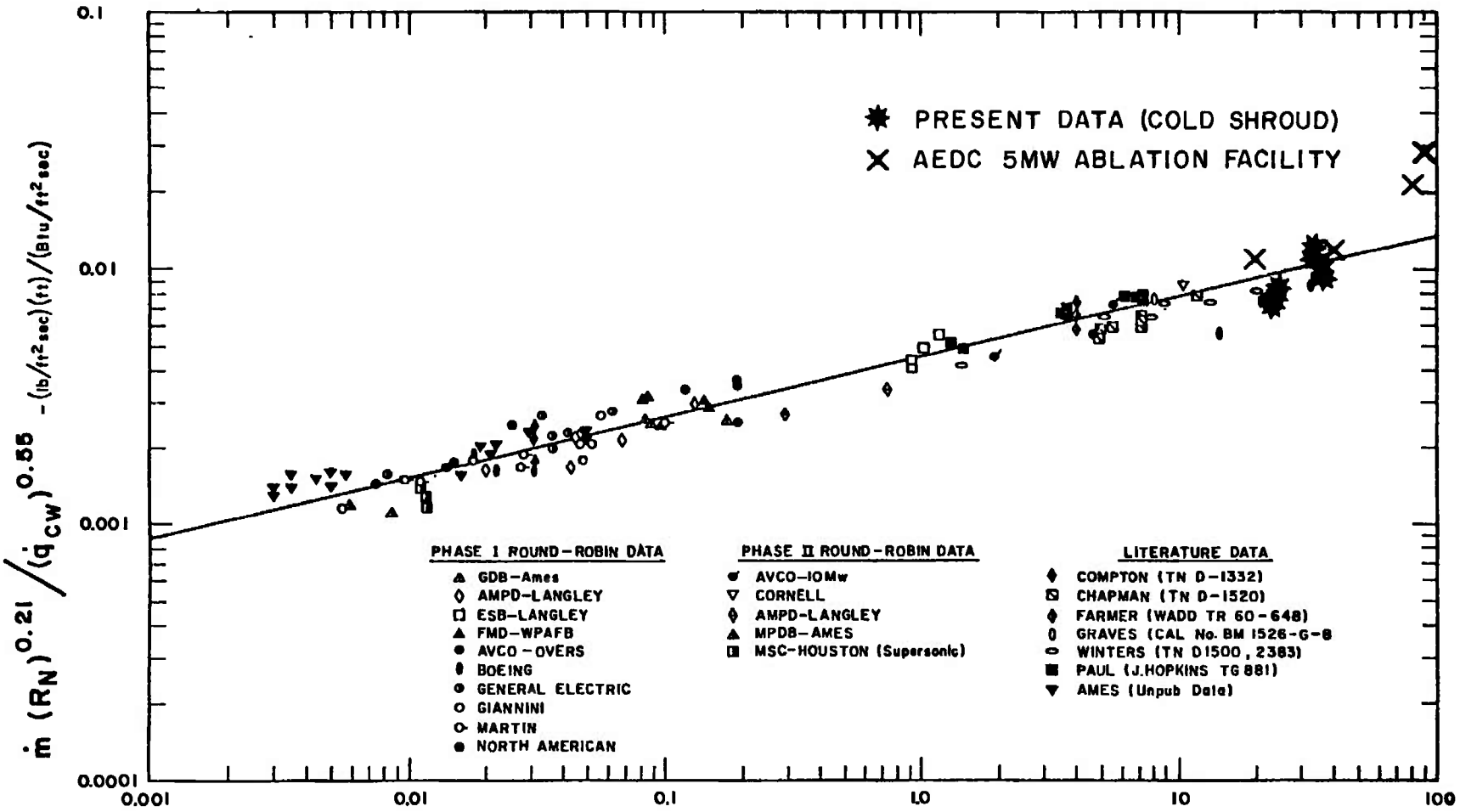

Fig. 39 Data of Ref. 9 Compared with Present Ablation Data

TABLE I
DATA COLLECTION LOCATIONS OF PRESSURE AND HEAT TRANSFER MODELS

PRESSURE MODELS

0.50-In. Radius Model	0.25-In. Radius Model	0.05-In. Radius Model
Orifice Location S/R_N	Orifice Location S/R_N	Orifice Location S/R_N
0	0	4.40
0.393	0.524	14.40
0.785	1.31	24.40
1.05	2.10	34.40
1.31	2.60	
2.10	3.80	
2.60	4.40	

HEAT TRANSFER MODELS

0.50-In. Radius Model	0.25-In. Radius Model	0.05-In. Radius Model
Gage Location S/R_N	Gage Location S/R_N	Gage Location S/R_N
0	0	4.40
0.785	1.05	14.40
1.05	2.10	24.40
1.31	3.80	34.40
2.10		

TABLE II
PROGRAM TEST CONDITIONS

Flow Properties	Test Condition					
	A	B	C	D	E	F
Shroud Pressure, psia	202	436	656	492	878	878
Arc Heater Pressure, psia	270	586	882	882	882	1177
Arc Heater Bulk Enthalpy, Btu/lbm	2450	2050	2000	2000	2000	1900
Stagnation Pressure Ratio, p_{o_H}/p_{o_C}	1.34	1.34	1.34	1.79	1.00	1.34
Free-Stream Static Pressure Ratio, $p_{\infty_H}/p_{\infty_C}$	1.00	1.00	1.00	1.34	0.75	1.00

TABLE III
COMPARISON OF ENTHALPY MEASURED BY VARIOUS MEANS

Extension	P_{o_H} atm	H_{HB} Btu/lbm	H_{ESF} Btu/lbm	$H_{oP_{avg}}$ Btu/lbm	$\frac{H_{oP_{avg}}}{H_{HB}}$	$H_{o_{calor}}$ Null	$H_{o_{calor}}$ Coax
0 ↓	16.43	2447	2127.2	2377 2265	0.973 0.926		2500
	41.18	1997	1889.7	1765 1713	0.891 0.858		3300 3300
	60.12	1991	1964.6	1603 1516	0.806 0.763		
	60.22	1961	1971.9	1898 1628	0.970 0.830		
	60.73	2109	1964.6	1782 1627	0.846 0.774		
0.80 ↓	17.86	2540	2122.1	2502 2433	0.990 0.965	3000 2760	3700 3070
	38.38	2087	1971.9	1890 1918	0.909 0.920		
	58.28	2042	1964.6	1683 1567	0.824 0.768		
	58.18	2065	1976.8	1698 1605	0.820 0.778		
	57.83	1978	1976.8	1524 1565	0.772 0.794		
	80.33	1843	1702.4	1276 1195	0.693 0.647	2200 2150	2150 2700
1.60 ↓	20.29	2193	1928.1	1985 1840	0.908 0.840	2750 2600	3500 3050
	39.76	2055	1875.5	1420 1795	0.692 0.675	2450 2625	2560
	60.14	2069	1911.3	1526 1486	0.740 0.720	2600 2700	2100 2300
	60.07	2084	1942.7	1626 –	0.782 –		
	59.91	2097	1971.9	1400 1411	0.674 0.674		

UNCLASSIFIED

Security Classification

DOCUMENT CONTROL DATA - R & D

(Security classification of title, body of abstract and indexing annotation must be entered when the overall report is classified)

1. ORIGINATING ACTIVITY (Corporate author)	2a. REPORT SECURITY CLASSIFICATION
Arnold Engineering Development Center, Arnold Air Force Station, Tennessee 37389	UNCLASSIFIED
	2b. GROUP N/A

3. REPORT TITLE

FURTHER EVALUATION OF A NEW FACILITY CONCEPT FOR TESTING LARGE ABLATION MODELS AT HIGH STAGNATION PRESSURES

4. DESCRIPTIVE NOTES (Type of report and inclusive dates)

July 1, 1970 to June 30, 1971--Final Report

5. AUTHOR(S) (First name, middle initial, last name)

R. T. Smith and J. C. Pigott, ARO, Inc.

6. REPORT DATE	7a. TOTAL NO. OF PAGES	7b. NO. OF REFS
October 1971	70	9

8a. CONTRACT OR GRANT NO.	9a. ORIGINATOR'S REPORT NUMBER(S)
b. PROJECT NO. 8950	AEDC-TR-71-212
c. Program Element 62201F	9b. OTHER REPORT NO(S) (Any other numbers that may be assigned this report)
d.	ARO-PWT-TR-71-153

10. DISTRIBUTION STATEMENT

Approved for public release; Distribution unlimited.

11. SUPPLEMENTARY NOTES	12. SPONSORING MILITARY ACTIVITY
Available in DDC	Arnold Engineering Development Center (XON), Air Force Systems Command, Arnold AF Station, Tenn.

13. ABSTRACT

This report presents the results of the third phase of an investigation to determine the feasibility of extending ablation test facility capability by surrounding the high enthalpy flow with a coaxial cold jet. The technique was applied to the 5-MW arc heated facility at pressures up to 80 atm. A variety of data probes and models were used to determine flow-model interactions. Final results show the technique to be excellent for simulating flow over very large ablation models.

DD FORM 1 NOV 65 1473

UNCLASSIFIED

Security Classification

14. KEY WORDS	LINK A		LINK B		LINK C	
	ROLE	WT	ROLE	WT	ROLE	WT
1 arc heaters						
2 ablation						
test facilities						
enthalpy						
pressure						
flow fields						
reentry						
probes						
flow visualization						
3 ablation test facilities						

AFSC
Arnold AFS Tenn